Aus der Klinik für Neurochirurgie
der Heinrich-Heine-Universität Düsseldorf
Direktor: Univ.-Prof. Dr. med. Hans-Jakob Steiger

Experimental investigation of photodynamic diagnostic and therapy on a human chordoma cell line model *in vitro*

D I S S E R T A T I O N

zur Erlangung des Grades eines Doktors der Medizin
der Medizinischen Fakultät der Heinrich-Heine-Universität
Düsseldorf

Vorgelegt
von Lennert Eismann
2019

Als Inauguraldissertation gedruckt mit der Genehmigung der Medizinischen Fakultät der Heinrich-Heine Universität Düsseldorf

Gez.:

Dekan: Univ.-Prof. Dr. Nikolaj Klöcker

Erstgutachter: PD Dr. Jan F. Cornelius

Zweitgutachter: Prof. Dr. Martin Wagenmann

Teile dieser Arbeit wurden veröffentlicht:

Jan F. Cornelius, Lennert Eismann, Lara Ebbert, Brigitte Senger, Athanasios K. Petridis, Marcel Alexander Kamp, Rüdiger V. Sorg, Hans Jakob Steiger, 5-Aminolevulinic acid-based photodynamic therapy of chordoma: In vitro experiments on a human tumor cell line, In Photodiagnosis and Photodynamic Therapy, Volume 20, 2017, Pages 111-115

Zusammenfassung

Chordome sind seltene Tumore der Schädelbasis und des Os sacrum. Charakteristisch ist ihr langsames infiltratives Wachstum, weshalb diese Tumore meist erst im fortgeschrittenen Stadium symptomatisch werden. Der Goldstandard in der Therapie ist eine möglichst radikale Resektion gefolgt von einer adjuvanten Bestrahlung. Aufgrund von später Diagnosestellung und der Nähe zu vitalen Strukturen ist eine komplette Resektion schwierig und nur selten möglich. Residuales Tumorgewebe erhöht die lokale Rezidivrate. Chemotherapeutika zeigten bisher noch keinen Erfolg, sodass neue adjuvante Therapiemöglichkeiten notwendig sind. Eine alternative Behandlungsmethode könnte die 5-Aminolävulinsäure gestützte photodynamische Therapie darstellen, die bisher vielversprechende Ergebnisse bei unterschiedlichen Hirntumoren gezeigt hat.

In der vorliegenden Arbeit untersuchten wir das Potential von 5-ALA gestützter PDT an einer humanen Chordomzelllinie in einem *in vitro* Modell. Dabei konnten wir im Vergleich zur Standardinkubationszeit von 4 Stunden eine erhöhte dosisabhängige Fluoreszenz nach 6 stündiger Inkubationszeit beobachten. Zudem verzeichneten wir einen letalen Effekt 24 h nach Bestrahlung mittels Laserlicht der mit 5-ALA behandelten Zellen. Eine hohe Zelldichte konnte dabei als positiver Einflussfaktor für einen maximalen letalen Effekt identifiziert werden. Dies könnte Hinweis auf eine hohe interzelluläre Kommunikation und die Existenz eines sogenannten Bystander Effekts sein.

Diese Ergebnisse weisen erstens auf einen möglichen klinischen Nutzen von 5-ALA zur fluoreszenz-gestützten Resektion von Chordomen hin. Weiterhin könnten inoperable Tumorreste mittels photodynamischer Therapie adjuvant im gleichen Setting mit behandelt werden.

Weitere Untersuchungen an Zelllinien und Tumorgewebe sind allerdings nötig, um diese vielversprechenden ersten experimentellen Ergebnisse weiter abzusichern.

Summary

Chordomas are rare neoplasm of the axial skeleton with predilection for the skull base and sacral region. Patients become symptomatic at advanced tumor stages due to slow and infiltrative growth into adjacent anatomical structures. At present, standard therapy is radical resection followed by radiotherapy. However, late diagnosis and proximity to surrounding vital structures often result in subtotal excision and hence in elevated local recurrence rates. Up to date, chemotherapy has shown to be ineffective. Therefore, new adjuvant treatment modalities are needed. 5-aminolevulinic acid based photodynamic therapy revealed promising results in meningioma, glioma and puitary adenoma models and encouraged us to investigate the efficacy of ALA/PDT on a human chordoma cell line *in vitro*.

The results indicated that PPIX accumulation was superior after 6 h 5-ALA incubation time in comparison to a standard incubation time of 4 h. Furthermore, we detected a lethal effect 24 h of laser-irradiation on chordoma cells having been incubated for 6 h with graded doses of 5-ALA beforehand. High cell density of chordomas increased toxic effect of ALA/PDT. This might be explained by high intercellular communication and suggests existence of a so-called bystander effect.

These preliminary findings of PPIX accumulation after exogenous 5-ALA application in chordoma cells may be of clinical interest for fluorescence-guided surgery of chordomas. In fact, residual tumor might better be detected increasing local tumor control. Even more, unresectable tumor remnants might be destroyed by ALA/PDT as intraoperative adjuvant treatment modality.

Further investigations on different chordoma cell lines and tumor cells are needed to confirm these preliminary findings.

Abbreviations

5-ALA	5-aminolevulinic acid
ALA-DH	Aminolevulinate dehydratase
ALAS	Aminolevulinic synthase
ALA/PDT	5-aminolevulinic acid based photodynamic therapy
AMPK	AMP-activated protein kinase
APAF	Apoptotic protease-activating factor-1
CT scan	Computed tomography scan
CSF	Cerebrospinal fluid
DC	Dendritic cell
EGFR	Epidermal growth factor receptor
ER	Endoplasmatic reticulum
FACS	Fluorescence activated cell sorting
FBS	Fetal bovine serum
FC	Ferrochelatase
IMDM	Iscove's modified dulbecco's medium
ISC	Intersystem crossing
LEDs	Light-emitting diodes
MAM	mitochondria-associated ER membrane
MFI	Mean fluorescence intensity
MRI	Magnetic resonance imaging
NO	Nitric oxide
PBG	Porphobilinogen
PBGD	Porphobilinogen deaminase
PBS	Phosphate buffered saline
PDD	Photodynamic diagnostic
PDT	Photodynamic therapy
PFS	Progression free survival

PPIX	Protoporphobilinogen IX
PS	Photosensitizer
RFS	Recurrence-free survival
ROS	Reactive oxygen species
SEER	Surveillance, Epidemiology and End Results Program
SEM	Standard error of the mean
TUR	Transurethral resection

Table of Contents

1 Introduction

1.1 Chordoma

Chordoma is a rare malignancy with an incidence of 0.08-0.5/100.000 person per year (1, 2) and a predominance in males (3, 4). It is presumed that this entity arises from remnants of the embryonic notochorda along the axial skeleton with a preferred location in the sacral and skull base regions (5-7). Histologically, chordoma is classified into three subtypes: classical, chondroid and dedifferentiated (8, 9). The most common subtype is the classic, whereas in only 5 % of patients the most aggressive, dedifferentiated form is documented (10, 11). Chordomas present heterogeneity of cells. El-Heliebi, A., et al. revealed three different types of chordoma cells: Small non-vacuolated spindle cells, which develop through an intermediate cell status with small vacuoles to the typical huge physaliferous cells with large vacuoles (12). The tumor appears in cluster cell formation separated by fibrous septa and enveloped in a myxoid stroma (8, 13).

Chordomas are considered as low-grade malignant neoplasm and with a slow growth pattern causing late symptoms, when tumor compresses surrounding anatomical structures (10, 14, 15).

Median age at diagnosis of chordomas is 60 years, but skull base chordomas tend to arise in younger patients (13). Depending on tumor localization first symptoms are often very unspecific (11). Most common in sacrococcygeal chordomas is low back pain and headache or palsies of the cranial nerves in the skull base (16).

Appearance in diagnostic computed tomography scan (CT scan) is hypodense and often with invasion of bony structures (17). Magnet resonance imaging (MRI) is more precise than CT scan in detecting tumor expansion (17). Typically, MRI appearance of chordomas is moderately hypointense in T1-weighted and slightly hyperintense in T2-weighted sequences even though there is a high diversity (5, 17).

Late diagnosis makes surgical treatment challenging, especially preserving surrounding vital structures (15). The gold standard is radical excision for best local tu-

mor control (11). In curative surgery, negative resection margins should be intended (18). Particularly in skull base chordoma *en bloc*-excision and R0 resection is often impossible due to proximity of cranial nerves, carotid artery and other vital structures (15). Nevertheless, cyto-reduction is also important for effective postoperative radiation (18). Endoscopic endonasal surgery has been established as an efficient and minimal invasive approach for chordomas located in the clivus (14, 19-21). Frequently reported perioperative complications in chordomas located in the craniocervical junction are cerebrospinal fluid (CSF) leakage with a range from 5 - 35.3 % (6, 22), neurological deficits 28.6 - 29.4 % (22, 23) and meningitis 5 - 17.6 % (6, 22). The rates depend on different surgical approaches, techniques and a variety of tumor extensions and volumes.

Resection of chordomas located in the os sacrum is generally highly invasive due to large tumor volume at the time of diagnosis (24). Surgery of chordomas involving the low and mid-sacral region may preserve the sacroiliac joint and are associated with better neurological outcomes (24). Postoperative impairment of intestinal and urinary function are reported in 12.5 % of the cases with surgery in low-sacral region and 75 % in mid-sacral region, respectively (24). Almost all patients who undergo high sacrectomy suffer of gastrointestinal and urinary symptoms postoperatively (24).
In the rare case of chordomas involving the mobile spine total spondylectomy is the most effective treatment to achieve negative margins (25).

Intraoperative tumor rupture should be prevented in order to avoid cell seeding along the surgical pathway (14, 15). Arnautovic et al. report a surgical seeding rate of 7.3 % in chordoma surgery (26). In regard of cell seeding, the use of preoperative biopsy to determine the diagnosis is questionable (11, 27). Nevertheless, fine needle aspiration biopsy has been reported to be the most adequate technique to obtain tissue samples (11, 15, 28). Biopsy or surgical pathway should be included in definite treatment as surgery or adjuvant radiation therapy to prevent local recurrence due to cell seeding (11).

Degree of surgical resection in chordomas of the os sacrum determines time to local recurrence, which is 8 months after subtotal excision compared to 2.27 years after gross total resection (15). Similarly, progression-free survival (PFS) for skull base chordomas is 68.9 months after extended surgery in comparison to 34.1 months after intralesional resection (29). Despite surgical advancements *en bloc* excision is feasible in half of sacral and even less in spine and skull base chordomas and consequently recurrence is very frequent (15). The 5-years recurrence-free survival (RFS) in skull base chordomas is 41 % after single or multiple treatments (30). In spinal chordomas the 5-year RFS is 58.4 % (31) after *en bloc* resection. A study of sacral chordomas treated with surgery reported a 5-year-local-relapse rate of 30 % (32).

Due to insufficiency of surgery as monotherapy in the treatment of chordomas adjuvant treatment modalities are frequently used.

No approved effectiveness and recommendation of chemotherapy for the treatment of chordomas has been described (11, 15). Nevertheless, an *in vitro* model showed a sensibility to Doxorubicin, Trabectedin (Yondelis), PM1004 (Zalypsis), and Cisplatin (33). Gini F. Fleming et al. reported two cases of dedifferentiated sacral chordomas obtaining complete remission after chemotherapeutical treatment with Ifosfamide (34). A phase-II trial tested the effect of Topoisomerase inhibitor in 15 patient with chordomas (35). In less than 10 % of the patients a response was observed and time to disease progression could be prolonged (35). Based on these results chemotherapy remains a controversially discussed adjuvant treatment option.

Recently molecular targeted therapy has become a new focus of anti-cancer research. The inhibition of the tyrosine-kinase pathways is known to positively affect multiple signalling pathways in malignancies (36). For instance, some studies have reported an effect of tyrosine-kinase inhibitor in chordomas (37, 38).

Tyrosine-kinase inhibitors affect different pathway receptors such as vascular endothelial growth factor (VEGF), platelet-derived growth factor and KIT-pathway (36). The interception of the mentioned pathways was described to improve patient's burden of symptoms and post-treatment imaging showed decreased contrast enhancement and liquefaction of tumor tissue (37, 38). Furthermore, the use of inhibit-

ing the tyrosine-kinase of the epidermal growth factor receptor (EGFR) in treatment of resistant chordomas was described in a case report with a favourable outcome (39). However, there exists no standardized systemic adjuvant therapy recommendation for chordomas so far.

The mainstay of adjuvant treatment is postoperative high-energy radiotherapy (40). In 1982, Suit et al. disclosed the efficacy of proton beam therapy for chordomas (41). The adjuvant radiation therapy delayed local relapse compared to surgical monotherapy (42). In cases of complete tumor resection the use of postoperative radiotherapy is still controversially discussed (42, 43). Using photon or proton beam with classic fractions a minimum dose of 74 GyE is needed (18). Radiation with doses lower than 60 Gy have been reported to show poor local tumor control (44). In palliative care, low-dose radiotherapy may be profitable for short term local tumor control (18, 45).

The described rates of distant lesions at the time of initial diagnosis varies from 5 % to 65 % (15). The median time to develop metastasis during disease is 4.8 years after diagnosis (46). Typical sites of metastases are lungs, soft tissue and bones (46).
According to the *Surveillance, Epidemiology and End Results Program* (SEER) database the median survival is 6.29 years (15). 5-year, 10-year survival rates are 67.6 % and 39.9 %, respectively (15).

1.2 Medical use of photochemical reactions

Photodynamic therapy (PDT) is a minimal invasive anticancer treatment known for over a hundred years, but has recently gained more attention (47-49).
The toxic effect caused by the interaction of a chemical reagent and light has first been described on a species of paramecium in 1900 by. O. Raab (49). In 1975, Dougherty et al. achieved the historical breakthrough in photodynamic therapy (50). He reported cure of various tumors in mice and rats by using hematoporphyrin and red light irradiation (50). Nowadays clinical use of PDT is well reported as anti-

cancer treatment for mesothelioma (51), lung cancer (52), oral cancer (53, 54) and bladder (55). Also first clinical experiences exist for some brain tumors (56, 57).

The procedure consists of two stages: first stage is the application of a non-toxic dye, which is called the photosensitizer (PS). Due to metabolic differences in dysplastic or neoplastic cells the photosensitizer specifically accumulates in the targeted tissue. After a specific incubation time, when the PS concentration is maximum, stage two is performed: the irradiation. Application of light with a specific wavelength according to the applied PS leads to a biochemical cascade resulting in the release of radical oxygen species (ROS) inducing apoptosis or necrosis (47).
PDT is approved in combination with radiation therapy showing additive treatment effects (58). Pogue et al. reports even an increased therapeutic effect of radiotherapy and PDT using the PS verteporfin (59). Also several combinations of PDT with different chemotherapy pharmaceutics were reported (60). Some poly-therapy schemes report an enhanced efficacy of chemotherapy and PDT (61, 62). Moreover, no carcinogenic impacts are known of accumulation of PS in cells (47).

1.2.1 Photosensitizer

Photosensitizers are synthetic or naturally produced reagents with the ability to transfer light energy (63). Substrates considered to be a PS have to fulfil activation of a photochemical reaction when illuminated with light of appropriate wavelength (63). The inert PS receives energy via photons and proceeds to a high-energy status (63). The activated PS tends to return to a low-energy status and emits energy in different ways such as fluorescence or photochemical reactions (63).
For clinical use in patients additional conditions are necessary like non-toxicity, tolerable side effects, accumulation in target tissue, easy application and commercial availability (63).

5-Aminolevulinic acid (5-ALA) is a commonly used physiological precursor of the PS protoporphyrin IX (PPIX) (47). 5-ALA and PPIX are intermediate metabolites of the heme-biosynthesis. Beside its function in hemoproteins almost all mammal cells are

capable to produce heme, which also is fundamental in protein metabolism and cell differentiation (64).
The aspects of high cellular 5-ALA uptake, increased synthesis of PPIX and reduced conversion to heme allow a selective accumulation of PPIX in malignant tissue (65). In addition, a high photoactivity makes PPIX an useful PS (64).

In clinical settings non-active 5-ALA is applied either topically (66), orally or intravenously (53, 67) injected before it reaches the target tissue where 5-ALA is metabolized to the active PS PPIX (63).
5-ALA is eliminated with a plasma half-life of 50 mins after intravenous and 45 mins after oral application (64). Unfavorable pharmacokinetics are high unchanged renal excretion and metabolic first-pass effect (68).
The hydrophilic nature of 5-ALA hinders diffusion through membranes and deep penetration of the target tissue (69). This shortcoming led to researches in modifying 5-ALA for better efficiency doses (64). Esterification of 5-ALA increases the lipophilicity and consequently the local bioavailability (64). Therefore lower drug doses can be used to achieve equivalent results (64).

Heme biosynthesis starts in the mitochondria with the regulated formation of glycin and succinyl-CoA to 5-ALA catalyzed by 5-ALA synthase (ALAS) (see **Fig.1**) (64). 5-ALA itself underlays enzymatic cytosolic modification before re-entering the mitochondrial compartment (64). In the cytosol two molecules of 5-ALA are merged to porphobilinogen (PBG) (64). Consequently, PBG is formed in two further reactions to the cyclic porphyrin skeleton (64). Modifications in the cytoplasm and mitochondria produce PPIX before ferrochelatase (FC) introduces ferrous iron at the level of the inner mitochondria membrane (64). In a negative feedback loop heme regulates the pathway by controlling ALAS's mRNA half-life and enzymes transporting 5-ALA into the mitochondria (64). Application of exogenous 5-ALA circumvents this regulation mechanism (64).
Therefore the amount of 5-ALA-induced accumulated PPIX depends mainly on enzymatic activity of the heme bionsynthesis and intracellular 5-ALA content (65). Beside ALAS, which is bypassed by the exogenous application, porphobilinogen deam-

inase (PBGD) is the secondary rate limiting enzyme (65). Another favorable intrinsic characteristic for high PPIX accumulation is a low turnover by FC (65). Its metabolic rate highly depends on iron supply (65).

The tumor selectivity for PPIX accumulation may be explained by high porphobilinogen deaminase (PBGD) in contrast to low FC activity and low concentration of iron (70).

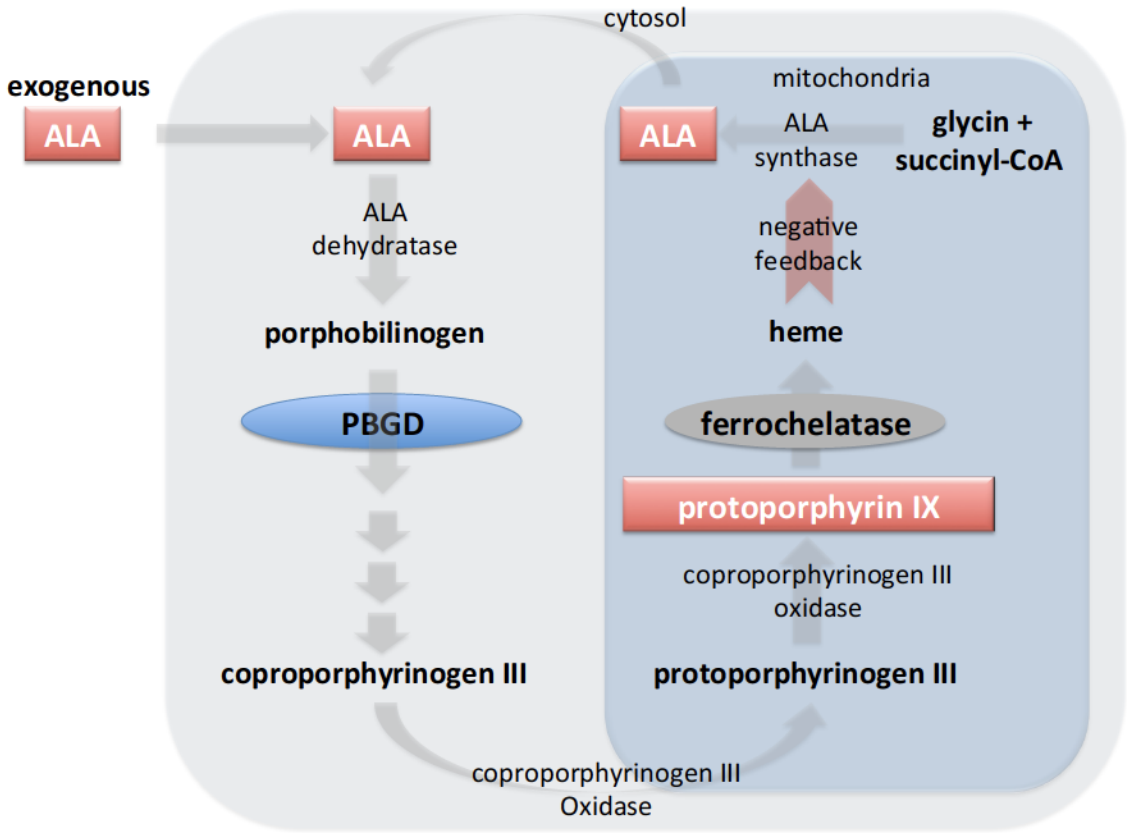

Fig. 1: Schematic illustration of exogenous 5-ALA application circumventing heme bionsynthesis' negative feedback loop:
After exogenous application 5-ALA enters cytosol and is metabolized like intrinsic 5-ALA to porphobilinogen. Subsequently heme bionsynthesis continues via the limiting enzyme porphobilinogen deaminase (PBGD). Further steps allow entry into mitochondria where protoporphyrin IX is produced. The last step introduces iron catalyzed by ferrochelatase. The amount of heme controls the feed-back mechanism (Adapted from Fotinos et al. (64))

1.2.2 Illumination

Any PS requires specific radiation conditions in wavelength and intensity to be activated (63). Short wavelength light activates more superficial tissues in comparison

with longer wavelengths, which may penetrate deeper into tissue (63). By adequately choosing PS and light wavelength this may increase possible tissue depth of PDT (63). Wavelength to a maximum of 800 nm may provoke production of singlet oxygen (47). Wavelengths above 800 nm transmit deficient energy and launch a photodynamic reaction (47).
Clinically, light of varying wavelength is commonly not used. Most frequently red light with a wavelength of 630 nm is utilized that penetrates tissues up to 0.5 cm (63).
Many of clinically applied PS such as 5-ALA can be activated by a wide spectrum of wavelength (63). Depending on localization of target tissue various light sources and distribution applications are available (63). Laser light has been proofed to be highly reliable but is expensive (63). New light emitting diodes (LEDs) enable longer treatment settings at lower costs (63).

1.2.3 Photochemical reaction

There are two relevant photochemical reactions in PDT so-called Type I and Type II reaction.

In Type I reaction the PS is configured in an excited triplet state and loses energy by transferring electrons to molecules in its direct surroundings (71). Thereby anions and cations are formed and may react with oxygen to produce ROS (71). In this process superoxide anions or subsequently hydrogen peroxide and hydroxyl radicals are generated (71). Hydrogen peroxide and hydroxyl radicals can easily pass through cell membranes and damage other cell compartments (71).

It is assumed that the Type II reaction is more relevant in PDT (63, 71). Type II reaction starts from the same excited triplet state of the PS as the Type I reaction. In contrast to the Type I reaction in Type II reaction energy is shifted to molecular oxygen without transferring electrons (71). The molecular oxygen is now transformed to highly reactive singlet oxygen: $^1O_2$ (47, 63, 71). Therefore, the high responsiveness of singlet oxygen reveals its destructive potential in the proximity of the PS (47).

For both reactions it is important that the PS is configured in the excited triplet state (71). In general PSs contain two paired electrons which rest in the energetically low-

est orbital (47, 71). This status is called the ground state (47, 71). Illumination of the PS leads to transfer of electrons in energetically higher orbital positions, the excited singlet state (71). Due to the nature of the electrons they desire to reach its more favourable ground state again (71). This can occur by losing energy via fluorescence or heat (71).

A characteristic of PS is the high probability to undergo an alternative way from the excited singlet state to a long-lasting configuration, the triplet state (71). This iso-energetic process is described as intersystem crossing (71). The triplet state is defined as two unpaired electrons and with the same spin (71). The PS in its triplet state can drop to its energetically lower ground state by going through phosphorescence and the described photochemical reactions Type I and II (71).

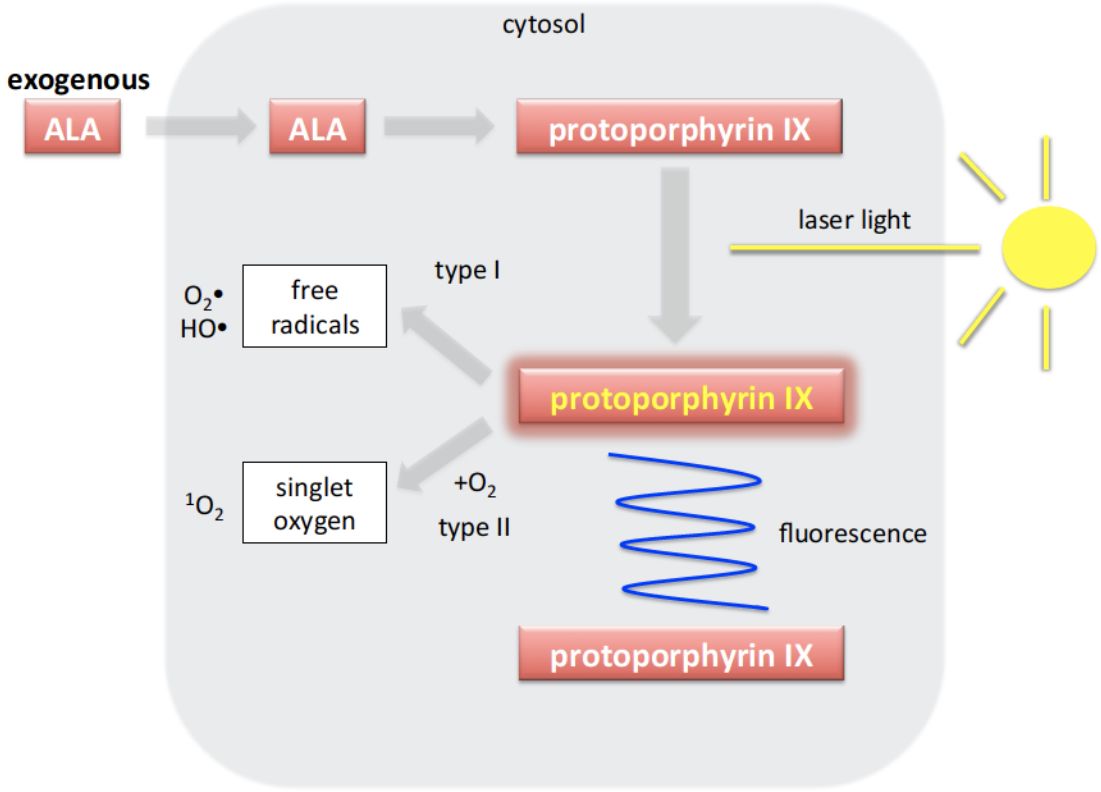

Fig. 2: Schematic illustration of photochemical reactions of 5-ALA/ protporphyrin IX.
After exogenous 5-ALA application protoporphyrin IX (PPIX) accumulates and is activated by laser light. The excited PPIX can react in two different photochemical reactions to free radicals (Type I) or to singlet oxygen (Type II). Both high reactive products may provoke cell death. A third option of excited photosensitizer to release energy is via fluorescence emission. (Adapted from Wachowska et al. (72))

1.2.4 ALA/PDT induced cell death

In ALA/PDT generated oxidative stress leads to destruction of different cell compartments. Its extent determines the cellular impact (73). The programmed cell death, called apoptosis, must be distinguished from necrosis with onset of inflammatory reactions and from a simultaneous pathway, autophagy, which can also end in cell death (73).

Light dose and PS concentration in the target cells determine the extent of ROS and hereby the type of cell death (63). Deeper tissue regions with lower oxidative stress preferentially undergo apoptosis and/or autophagy whereas superficial cells create a high amount of reactive oxygen and follow the necrotic pathway (63, 73, 74).

In photochemical reactions produced singlet oxygen is very limited in its reaction radius (10-55 nm in cells) and its lifetime (10-320 ns) (47). Accordingly, cell damage will occur very close to the PS molecule in the cell (47). 5-ALA, which accounts to the group of porphyrins usually accumulates at cell membranes (73).

Most relevant pathway in PDT induced cell death is apoptosis (47, 73).

Apoptosis can be initiated by several mechanisms via cell membrane receptor, mitochondrial system, T-cell or NK-cell associated or using the sphingomyelin-cermaid pathway (73).

Mitochondrial membrane damage evoked by ALA/PDT can lead to the release of pro-apoptotic caspase activators via Bcl-2 membrane proteins (47, 75). This required event is called *the mitochondrial outer membrane permeabilization* to activate the intrinsic pathway of apoptosis (76).

Cytochrome c diffuses like other caspase activators from the mitochondrial intermembrane space into the cytosol to act as co-factor for the apoptotic protease-activating factor-1 (APAF-1) (76). APAF-1 and cytochrome c trigger the initiator caspase-9 and form an apoptosome (77). Subsequently effector caspases-3 and -7 are activated that present the common apoptotic pathway of extrinsic and intrinsic influence (77).

In cell morphology apoptosis is described as cell-shrinkage, chromatin condensation and plasma membrane blebbing (75). The apoptotic cell passes through a round

appearance with darkened cytosol and condensed chromatin to apoptotic cell fragments, which are finally phagocytosed by macrophages (75).

PDT toxicity is not only mediated by apoptosis but a fraction of treated cells also undergoes necrosis (47, 69). For a long time necrosis was described as uncontrolled decay of cells, but recent studies have revealed that some forms of necrosis follow a signal transduction pathway (78).
Necrosis can either be induced via death receptors or more relevant in ALA/PDT again via ROS (78). Oxidative stress provokes DNA damage, mitochondrial dysfunction, lipid peroxidation that further leads to destabilization of plasma membranes (78).
Cells which undergo necrosis swell and take a round form until membranous disintegration occurs (79). Release of cytosolic contents and proinflammatory mediators into the extracellular matrix explain the associated inflammation (79).

The third relevant cell death pathway is autophagy that describes the degradation of cellular components in a double membranous autophagosome ending in a maximum extent in self-digestion (80).
In cases of different physiological stress situations such as nutritious shortage, DNA damage or hypoxia autophagy can occur (80). In autophagy, dysfunctional cell organelles or proteins are re-cycled to provide energy and to allow short-term survival (80, 81). Thus autophagy represents either a cytoprotective mechanism to stand by nutrients deficiency or delays apoptosis in prolonged shortages or leads to autodigestion if cell is further exposed to extensive stress (80).
In ALA/PDT mitochondrial damage results in a decrease of ATP and activates AMP-activated protein kinase (AMPK) (81). AMPK has been shown to induce autophagic cell death (81).

Besides these direct mechanisms to induce cell death ALA/PDT deploys further antitumor effects. Photodynamic therapy leads to vascular occlusion of tumor vessels and enhances immune reactions (82).

The combination of perishing tumor cells, the release of vasoactive molecules and damage of endothelial cells explains decelerated blood flow (82). Subsequent hypoxia and/or thrombosis impairs tumor tissue and its regrowth (82, 83).

The immunological reaction after ALA/PDT is mainly associated with T-cell reaction (84). ALA/PDT causes increased migration of neutrophils and release of pro-inflammatory cytokines (84). Fragments of destroyed tumor cells provide antigens to dendritic cells (DC) and discharge of stress proteins (84). Following maturation of DC occurs and leads to cytotoxic T-cells activation in the lymphatic system (84). Increased affinity of DCs to tumor cells and maturation following PDT was reported (84).

1.2.5 Photodynamic diagnosis

Photodynamic reaction can also be used in diagnostics. Therefore a PS, e.g. 5-ALA as described above, is applied to the patient and accumulates in the target tissue (85). After illumination with appropriate wavelength the PS reaches its singlet state and desires for its ground state (85). In contrast to PDT PS loses its energy by fluorescence emission and makes the target tissue visible (85). Usually cells emitting 5-ALA induced fluorescence appear bright red-pink when visualized with an appropriate optic system (e.g. microsope with special filters) (85, 86). Using this technique neoplastic cells which are difficult to distinguish from physiological tissue may be detected (85). In urology fluorescence detection is used to reveal carcinoma in situ in the bladder (85). Also in operative settings fluorescence-guidance is used to ensure negative tumor margins (85).

In neurosurgery fluorescence-guided surgery in glioma has become widely spread. Stummer et al. (2006) reported in a phase-III trial an increase of complete resection rate using 5-ALA from 35 % to 65 % (86). Accordingly, the 6 months progression free survival was 41 % vs. 21 % for patients resected under fluorescence guidance as compared to white light excision (86). Usually 5-ALA is applied orally 2.5-3.5 h before surgery (87). Intraoperative surgical microscopes are equipped with fluorescence imaging hardware. Thus fluorescing tumor tissue is visualized as bright red-pink color in comparison to physiological brain that appears dark blue or black (87). Intensity of fluorescence and surgeons' experience guides the extent of resection.

Recently, fibre optics have been developed for measuring fluorescence intensity and making assessment more objective (88). Until now meningiomas (89-91), childhood brain tumors (92-94) and metastases (95-97) have been reported to hold potential for fluorescence-guided surgery.

1.3 PDD and PDT as promising approaches in the treatment of chordomas

The difficult biological character of chordoma is challenging and patient outcome is still unsatisfying due to insufficient adjuvant treatment options.

High recurrence rates may be reduced by maximizing excision while preserving vital structures. This might be improved by fluorescence-guidance. Especially at the skull base prone to surgical complications, PDD might be useful to provide more safety for critical neuro-vascular structures.

Another clinical application could be the use of PDT in chordomas. Residual tumor which is unresectable or undetected tumor cells could be extinguished by ALA/PDT. The clinical practice of PDT allows even illumination of resection cavity of using the working channel of minimal invasive approaches (98). Its biological and histological features make chordomas an ideal target for PDT. Macroscopic appearance of chordomas is almost transparent. Microscopic character of chordomas shows large cells rich of vacuoles. This might allow deeper penetration of laser light.

2 Objective of this thesis

We investigated the promising treatment modality of 5-ALA based PDT on a human chordoma cell line. Based on established ALA/PDT protocols of our institute for glioma, meningioma and pituitary adenoma, we sought to investigate the chordoma cell line systematically:

1. Fluorescence activating cell sorting (FACS) was used to analyse PPIX accumulation after different incubation times and to evaluate graded doses of 5-ALA,

2. PDT sensibility was investigated for different 5-ALA concentrations by evaluating cell survival with spectrophotometry after treatment,

3. Cell cycle phase at the time of experiments was studied to elucidate the biological characteristics of this chordoma cell line.

First the laboratory investigations of intracellular accumulation of PPIX and sensibility of ALA/PDT in combination with the growth manner of this human chordoma cell line are reported. Secondly, the results and potential (pre-) clinical approaches of ALA/PDT as a new treatment modality of chordoma are discussed.

3 Material and Methods

3.1 Material

3.1.1 Human cell line

The immortalized human chordoma cell line U-CH2 was commercially available and purchased at Leibniz Institute DSMZ-German Collection of Microorganism and Cell Cultures. In 2010, Brüderlein S et al. isolated this cell line from a recurrent sacral chordoma of a 72 years old female patient (99).

For the present study no ethical approval was required as the experimental set-up was limited to an *in vitro* cell model and performed with a commercially available tumor cell line.

3.1.2 Chemicals and reagents

Product	Company	Country
Iscove's modified medium	GIBCO/Invitrogen	Ireland
RPMI 1640	GIBCO/Invitrogen	Ireland
Fetal bovine serum	Biochrom	Germany
GlutaMAX™ Supplement	GIBCO/Invitrogen	Ireland
ZellShield™	Minerva Biolabs	Germany
TrypLE™ Express Enzyme	GIBCO/Invitrogen	Ireland
Dulbecco's Phosphate Buffered Saline (PBS)	GIBCO/Invitrogen	Ireland
Dulbecco's Phosphate Buffered Saline (DPBS)	Sigma-Aldrich	USA
Trypan Blue solution 0.4 %	Sigma-Aldrich	USA
Aqua ad iniectablia	Braun	Germany
Cell Proliferation Reagent WST-1	Roche Diagnostics	Switzerland
ALA powder 500 mg	Merck	Germany
70% pure ethanol	Central pharmacy UKD	Germany
Muse™ Cell cycle reagent	Merck KGaA	Germany
Paraformaldehyde (PFA); 4 %	Affymetrix/USB	USA

Table 1: Chemicals and reagents

3.1.3 Consumables

Product	Company	Country
Cell Culture Flask T-75	Eppendorf AG	Germany
Conical Tubes 50 ml	Eppendorf AG	Germany
Safe-Lock Tubes, 1,5 ml	Eppendorf AG	Germany
96-well cell imaging plate, with lid, black with clear F-bottom, coverglass bottom	Eppendorf AG	Germany
Polypropylene Light Protection Tubes, conical bottom, brown	Greiner Bio-One	Austria
C-Chip, Neubauer counting chamber	NanoEnTek Inc.	Korea
Serological Pipettes, 10 ml, 20 ml, 50 ml	Eppendorf AG	Germany
ep Dualfilter T.I.P.S® 0,5-20 µl	Eppendorf AG	Germany
ep Dualfilter T.I.P.S® 20-300 µl	Eppendorf AG	Germany
ep Dualfilter T.I.P.S® 50-1000 µl	Eppendorf AG	Germany
ep Dualfilter T.I.P.S® 0,1-5 ml	Eppendorf AG	Germany
Eppendorf Combitips advanced®, 2.5 mL	Eppendorf AG	Germany
Eppendorf Combitips advanced®, 5 mL	Eppendorf AG	Germany
Glass pasteur pipettes	Brand GmbH + Co KG	Germany
Cryotube vialis	Nunc A/S	Denmark
Pipette tips (20 µl, 200 µl, 1000 µl)	Starlab	Germany
Plastic pipettes (5 ml, 10 ml, 25 ml)	Corning	USA
Polypropylene round-bottom tube (5 ml)	BD Biosciences	USA
Tissue culture flasks (T75, T175)	Greiner BioOne	Austria
Tube (15 ml, 50 ml)	Greiner BioOne	Austria

Table 2: Consumables

3.1.4 Medium

Medium with supplements

Iscove's Modified Dulbecco's Medium (IMDM) and RPM1640 in a ratio 4:1.

Supplements: 20 % FBS, 5 % Glutamax, 5 % Zellshield.

Medium without supplements

Iscove's Modified Dulbecco's Medium (IMDM) and RPM1640 in a ratio 4:1.

3.1.5 Instruments

Product	Company	Country
CO_2 Incubator	Binder GmbH	Germany
Flue work bench, Laminair, HA 2448	Heraeus Holding	Germany
Water bath WNB	Memmert GmbH + Co KG	Germany
Multipette	Heraeus, Sigma, Hettich, Sartorius	Germany
Eppendorf Research® plus pipette, 0,5-10 µL	Eppendorf AG	Germany
Eppendorf Research® plus pipette, 30-300 µL	Eppendorf AG	Germany
Eppendorf Research® plus pipette, 10-1000 µL	Eppendorf AG	Germany
Eppendorf Research® plus pipette, 0,5-5 mL	Eppendorf AG	Germany
Pipet controllers, accu-jet pro, electric	Brand GmbH + Co KG	Germany
Thermomixer comfort	Eppendorf AG	Germany
Fast Biotec TopStream 300	Fast Biotec Labortechnik	Germany
Muse™ Cell Analyzer	Merck KGaA	Germany
Laser, Ceralas, 635nm	Biolitec AG	Austria
Laser fiber, frontal diffusor	Medlight SA	Switzerland
Microplate Reader, Model 680XR	Bio-Rad Laboratories	Germany
Microscope CK-2TR	Olympus Europe	Germany
Microscope Eclipse TS	Nikon GmbH	Japan
Refrigerator	Liebherr-international Deutschland GmbH	Germany
Freezer	Liebherr-international Deutschland GmbH	Germany
Centrifuge 5810R	Eppendorf	Germany
CO_2 incubator CB210	Binder	Germany
CO_2 incubator Revco Ultima	Thermo Fisher Scientific	Germany
CO_2 incubator Thermo Forma	Thermo Fisher Scientific	Germany
CyAn ADP flow cytometer	Beckman-Coulter	Germany
Finnpipettes (10 µl, 50 µl, 200 µl)	Thermo Fisher Scientific	Germany
Multipipette (type M4 and *plus*)	Eppendorf AG	Germany
Pipette controller Acu-jet Pro®	Brand GmbH + Co KG	Germany
Pipette controller Pipetboy® acu	Integra Bioscience GmbH	Germany
Pipette controller Pipetus®	Hirschmann Laborgeräte	Germany
Pipettes Research *plus* (2,5 µl, 10 µl, 100 µl, 200 µl, 1000 µl)	Eppendorf AG	Germany

Tissue culture hood CleanAir CA/RE 4	CleanAir Techniek	Netherlands
Tissue culture hood Lamin Air 1.8	Thermo Fisher Scientific	Germany
Waterbath WNB22	Memmert	Germany

Table 3: Instruments

3.1.6 Softwares

Product	Application	Company
EndNote X7®	Reference management	Thomson
NIS-Elements BR	Microscope-software	Nikon GmbH
Mircrosoft Excel 2002	Analysis of PCR data	Microsoft
SPSS	Statistical analysis and visualization	IBM
Microplate manager	ELISA	Bio-Rad
Summit 5.2	Flow cytometry analysis	Summit 5.2

Table 4: Softwares

3.2 Methods

3.2.1 Cell culture

The cell line was treated based on the protocol of Bruderlein et al. (99) and modified as mentioned below. The U-CH2 cells were cultured in a humidified incubator at 37 °C under 5 % CO_2 atmosphere and maintained in Iscove's Modified Dulbecco's Medium (IMDM) and RPM1640 in a ratio 4:1 supplemented with 20 % FBS, 5 % Glutamax, 5 % Zellshield *(medium with supplements*). Passages were performed at a confluence rate of 95-100 % in a seven-day cycle. Therefore, medium was aspirated and cells were washed with 15 ml PBS. 10 ml TryplE was used to detach cells and incubated for 9 mins. Following TryplE was buffered with 10 ml new *medium with supplements* and cell suspension was carefully re-suspended. This 20 ml cell suspension was centrifuged at 37 °C, 1200 rpm for 5 mins in a 50 ml falcon tube. Subsequently, the suspension was aspirated and the cell pellet was carefully re-suspended with new 10 ml *medium with supplements*. This new cell suspension was split in a ratio 1:2 in new culture flasks. 30 ml *medium with supplements* were added to new culture flasks. After 3-4 days medium was aspirated, cells were washed by

15 ml PBS and 30 ml *new medium with supplements* was added. The doubling time was 7 days.

3.2.2 Experimental set-up of *in vitro* PDT

Cell harvesting

At 95-100 % confluence of cell layer the medium was aspirated. Cells were washed by 15 ml PBS and detached by regular cell culture protocol (see 3.2.1 cell culture). The 20 ml amount of cell suspension was administered into 50 ml Falcon tube and centrifuged at 37 °C, 1200 rpm for 5 mins. Medium was aspirated and cell pellet was carefully re-suspended with 5 ml new *medium with supplements*.

Cell counting

1 ml trypan blue was diluted with 1 ml PBS for staining the cells.

50 µl of cell suspension and 150 µl of trypan blue dilution was carefully re-suspended and used for cell counting. Cell counting was performed with the use of a Neubauer counting chamber (C-Chip, NanoEnTek Inc., Korea)

Cell seeding

Cells were harvested and kept in cell dilution. If needed further dilution was proceeded to achieve the favoured experimental cell density. The defined cell density was either 30.000 or 15.000 cells per well in a volume of 100 µl. An experimental 96-well plate was used and 22 wells were seeded with cells **(Figure 3)**.

Immediate cell seeding was performed to prevent cell settling. Multipette (Eppendorf AG, Germany) was used to fill the row of 6 wells from B3 – G3 and four quadruplets in the following positions with 100 µl defined cell suspension:

1. quadruplets B6, B7, C6, C7
2. quadruplets F6, F7, G6, G7
3. quadruplets B10, B11, C10, C11
4. quadruplets F10, F11, G10, G11

The wells from B3 – G3 were used for the standard extinction of untreated cells, therefore defined as ‘standard’. The four quadruplets were either used for experimental groups using different 5-ALA dilutions or served as negative control group (“radiation only” or “5-ALA only”). Additionally, a row of 6 wells from B2 – G2 was filled with 100 µl *medium with supplements* per well. These wells served to analyze extinction of *medium with supplements* only, defined as ‘blank’. To prevent evaporation outlined wells were filled with 200 µl of PBS. This positioning of experimental wells, ‘blank’ and ‘standard’ allowed a security distance of 2 wells to minimize scattered radiation.

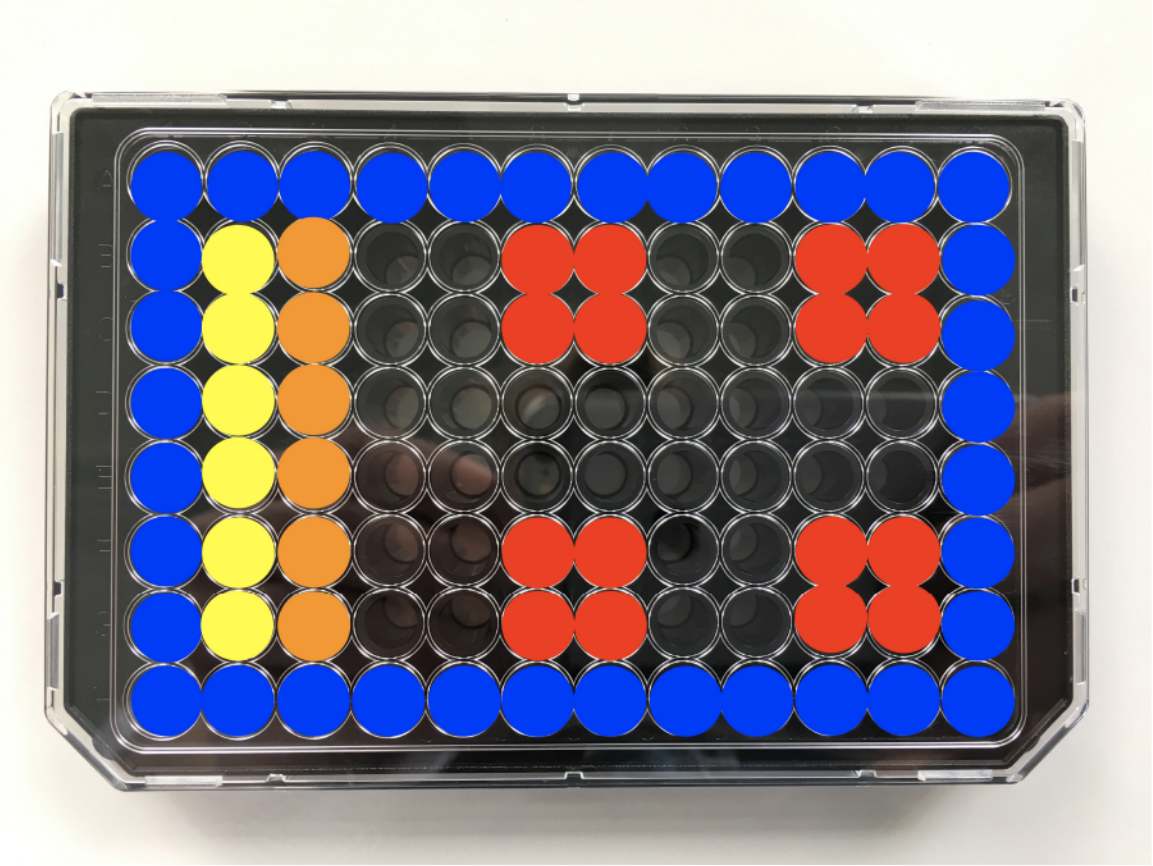

Fig. 3: Schematic illustration of the experimental 96-well plate
A light protected 96-well plate was used for experimental investigation of ALA/PDT. Blue colored wells were filled with 200 µl PBS to prevent evaporation. Yellow colored wells were used for extinction of 150 µl medium only and orange colored for untreated cells only. Red colored wells present the four experimental quadruplets. The distribution allows a two well safety distance to prevent scattered radiation.

Incubation after seeding

The seeded 96-well-plate was incubated for 12-18 h under regular culture conditions (in a humidified incubator at 37 °C under 5 % CO_2 atmosphere).

Dilution process of 5-ALA

500 mg 5-ALA-powder was diluted in a two-step procedure to achieve the experimental 5-ALA concentration. In a first step 500mg 5-ALA-powder was dissolved in 10 ml aqua ad iniectablia and in a second step dilution was performed with IMDM: RPMI1640 (4:1). 50 µl of the 5-ALA dilution was added to the experimental wells containing 100 µl of medium and cells. The final 5-ALA concentration in the wells was as indicated.

Each quadruplet contained one 5-ALA-dilution or was hold as negative control for radiation without 5-ALA, then 50 µl per well *medium without supplements* were added or a negative control of 5-ALA without radiation, then 5-ALA-dilution was added.

After administering the 96-well plate was shaken on the thermos-mixer at 37 °C, at 600 rpm for 2 mins.

ALA-incubation

Direct after 5-ALA-dilution or *medium without supplements* 96-well plate was incubated in the dark for 6 h under regular culture conditions (in a humidified incubator at 37 °C under 5 % CO_2 atmosphere).

Radiation

After cells were incubated with 5-ALA-dilution the 96-well plate was set in our radiation set-up and the quadruplets were radiated with a wavelength of 635 nm for 625 s and 1 W. The distance between laser probe and the bottom of the 96-well plate was 93 mm, which resulted in a fluence of 18.75 J/cm^2.

The order of radiation was: 1. Quadruplet -> 2. Quadruplet -> 4. Quadruplet -> 3. Quadruplet. Radiation was delivered at room temperature and in a non-sterile setting.

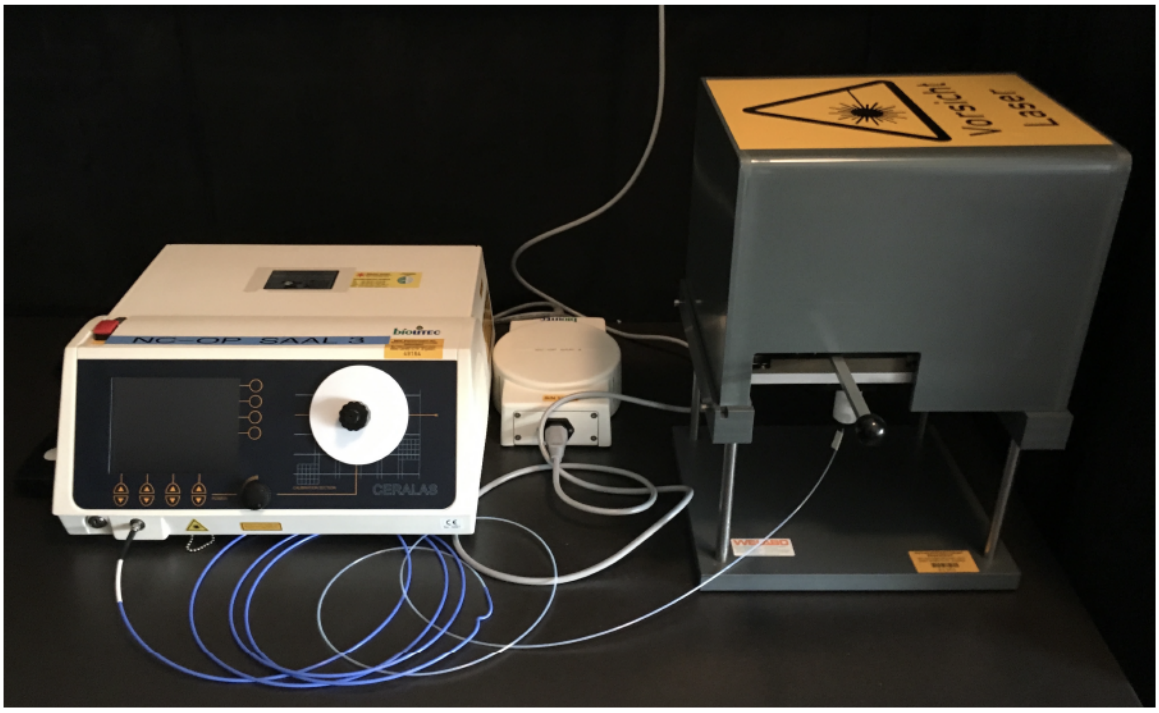

Fig. 4: Irradiation setup: Laser (left), fiberglass probe (blue), irradiation chamber for 96-well plate (right) .

Incubation Post-PDT

After radiation, the 96-well plate was stored for 24 h under standard culture conditions: in a humidified incubator at 37 °C under 5 % CO_2 atmosphere.

WST-1 Assay

Water soluble tetrazolium salt-1 (WST-1) assay is a cell proliferation reagent. The assay is based on the metabolism of tetrazolium salts to red coloured formazan by the mitochondrial dehydrogenases of viable cells. The amount of produced formazan corresponds to the quantity of viable cells. Spectrophotometry is used to quantify the amount of formazan dye at a specific wavelength by an ELISA reader (Microplate Reader, Model 680XR, Bio-Rad Laboratories, Germany).

In our experimental set up 24 h after radiation 15 µl per Well of WST-1 assay were added to the six blank wells, six standard wells and the experimental wells of the quadruplets.

Following the 96-well plate was mixed on the thermos mixer at 37 °C, 600 rpm for 6 mins. After the mixing procedure the 96-well plate was incubated under regular cul-

ture conditions (in a humidified incubator at 37 °C under 5 % CO_2 atmosphere) for 30 mins. Subsequently, the 96-well-plate was mixed again on the thermos mixer at 37 °C, 600 rpm for 6 mins. In direct series *WST-1 Assay readout* was performed in our ELISA reader and extinctions data were saved in Microsoft Excel.

Statistical analysis

Data was analyzed using SPSS statistics (Version 22 and 25, IBM, USA). For comparison of data, two-way ANOVA, Bonferroni's post-hoc multiple comparison test and the Mann-Whitney-U test were used. Unless stated otherwise, data are presented as mean ± standard error of the mean (SEM) for the number of experiments indicated.

Microscopic evaluation

Microscopic evaluation was performed during cell culturing, after cell seeding, before 5-ALA incubation, before WST-1 assay incubation and after WST-1 assay redout. Before 5-ALA-administration and after 24 h post radiation microscopic evaluation was performed and documented with the microscope-software (NIS-Elements BR, Nikon GmbH, Germany).

3.2.3 Fluorescence activating cell sorting

FACS was performed in cooperation with PD Dr. rer. nat. Rüdiger Sorg and Lara Ebbert of the Institute of Transplantation Diagnostics and Cell Therapeutics, Heinrich-Heine-University Düsseldorf.

Cell harvesting

Cells were harvested after 7-8 days culturing according the standard *cell harvesting* protocol mentioned in the methods chapter (*3.2.2) "Experimental set-up of in vitro PDT"*. Cells were counted and a cell concentration of 100.000 cells/ml was kept in a 50 ml falcon tube.

ALA-dilution process and incubation

5-ALA-dilution was performed according to the protocol mentioned above in chapter (*3.2.2) "Experimental set-up of in vitro PDT"*. Experimental groups of 100.000 cells/ml were incubated with concentrations of 0, 10, 20, 30, 40, 50 µg/ml of 5-ALA in *medium without supplements* for 4 h and 6 h. Incubation was under light protected standard culture conditions and terminated by a washing process using PBS.

Flow cytometry

Following the 5-*ALA-incubation* cells were fixed with 100 µl 4 % PFA. Cells treated with 0 µg/ml of 5-ALA served as negative control group. Flow cytometry was per-fomed using CyAn at LP 670/50 and the wavelength of excitation was 405 nm.

3.2.4 Cell cycle analysis

Cell harvesting

Cells were harvested as described in chapter (3.2.2) "Experimental set up of *in vitro* PDT" under the section 'cell harvesting'. Or cells were used from 'cell dilution' of ex-perimental set ups.

Cell washing

Cell dilution in a density of 500.000-1.000.000/ml were needed and contained in a 15 ml Falcon tube. Cell dilution was centrifuged for 5 min, 37 °C, 200 x G (1120 rpm) and subsequently supernatant was aspirated. 1 ml PBS was added to cell pellet and gently re-suspended. When reaching a homogenous cell dilution again centrifugation was performed according the same protocol (5 mins, 37 °C, 200 x G (1120 rpm)).

Cell fixation

Most of the supernatant was aspirated except for 50-100 µl that were left. Cell pellet was gently re-suspended in this dilution until reaching a homogenous cell dilution.
Cell dilution was taken up into pipette tip and slowly dripped in 1 ml, -20 °C cold 70 % ethanol under continuous agitation on the vortexer. Cells were fixated in -20 °C ethanol for at least 3 h.

Cell staining

200 µl of the fixated cell dilution was centrifuged for 5 mins, 37 °C and 300 x G. Supernatant was aspirated and 250 µl PBS was added to wash cells. Cell pellet was gently re-suspended until homogenous cell dilution was achieved. Again, centrifugation was performed according the same protocol (5 mins, 37 °C, 300 x G). Supernatant was aspirated and 200 µl of Muse cell cycle reagent was added and gently re-suspended. Cells were incubated for staining for 30 mins under light protection at room temperature.

Cell cycle read out

Stained cells were shaked using the vortexer and then read out by Muse™ Cell Analyzer.

Principle

Muse cell cycle reagent stains DNA of cells at different stage of cell cycle. The reagent is based on propidium iodide, which intercalates of DNA. According to cell cycle phase chromosomal content is synthesized in S-phase and is completely doubled in G2-phase. Based on this, fluorescence of cells in S-phase is higher compared to G1/G0-phase and cells in G2-phase are detected as even higher. By using RNAse A staining is more specific.

3.2.5 Statistical Analysis

For statistical analysis and plotting SPSS Statistics (version 22 and 25, IBM, USA) was used. Data were checked for normal distribution using Kolmogorov-Smirnov-Z and Shapiro-Wilk test. For comparison, multi-variant ANOVA and post-hoc Bonferroni tests were performed. Data are shown as mean ± standard error of mean (SEM) otherwise values are indicated. Significance was set for $p \leq 0.05$ and high significance for $p \leq 0.01$.

Statistical analysis and graphic illustration of results was performed in collaboration with PD Dr. rer. nat. Rüdiger Sorg and the Institute of Transplantation Diagnostics and Cell Therapeutics of the Heinrich-Heine-University, Düsseldorf as affiliation.

4 Results

4.1 FACS detected PPIX accumulation in chordoma U-CH2 cells

U-CH2 cell line was incubated with 0; 10; 20; 30; 40 and 50 µg/ml of 5-ALA, respecively. According to our institute's protocol for glioma, meningioma and pituitary adenoma cells were incubated for 4 h in group A and for 6 h in group B. Subsequently, cells were scanned by flow cytometry. In **Fig. 5** a representative sample of fluorescence detection is shown. Fluorescence intensity and the fraction of fluorescing cells were measured. **Fig. 6** displays the mean fluorescence intensity (MFI) of group A and B (n=7). **Fig. 7** shows the fraction of fluorescing cells in both experimental groups (n=7).

After exogenous 5-ALA application to U-CH2 cells PPIX accumulated dose-dependently in group A and B (ANOVA, $p < 0.0001$). There was no significant difference between group A and B for low concentrations of 10 and 20 µg/ml of 5-ALA. For higher concentrations ≥ 30 µg/ml of 5-ALA we found a significant increased MFI of group B (6 h incubation time) in comparison to group A (4 h incubation time) (ANOVA/Bonferroni's; $p \leq 0.05$). The fraction of fluorescing cells increased significant dose-dependently from 0; 10; 20; 30 µg/ml of 5-ALA in experimental group A (4 h incubation time) and simultaneously from 0; 10; 20 µg/ml in experimental group B (6 h incubation time) (ANOVA/Bonferroni's; $p \leq 0.05$). Higher 5-ALA doses reached a plateau from 40 µg/ml in group A and already from 30 µg/ml in group B. The fraction of fluorescing cells of group A and group B differed significantly for 0; 10, 20, 30; 40 µg/ml (T-test; $p \leq 0.05$). The prolonged incubation led to an earlier plateau of 30 µg/ml in comparison to 40 µg/ml in group A. The prolonged incubation time of 6 h led to larger fractions of fluorescing cells especially for lower 5-ALA concentrations **(Fig. 7)**.

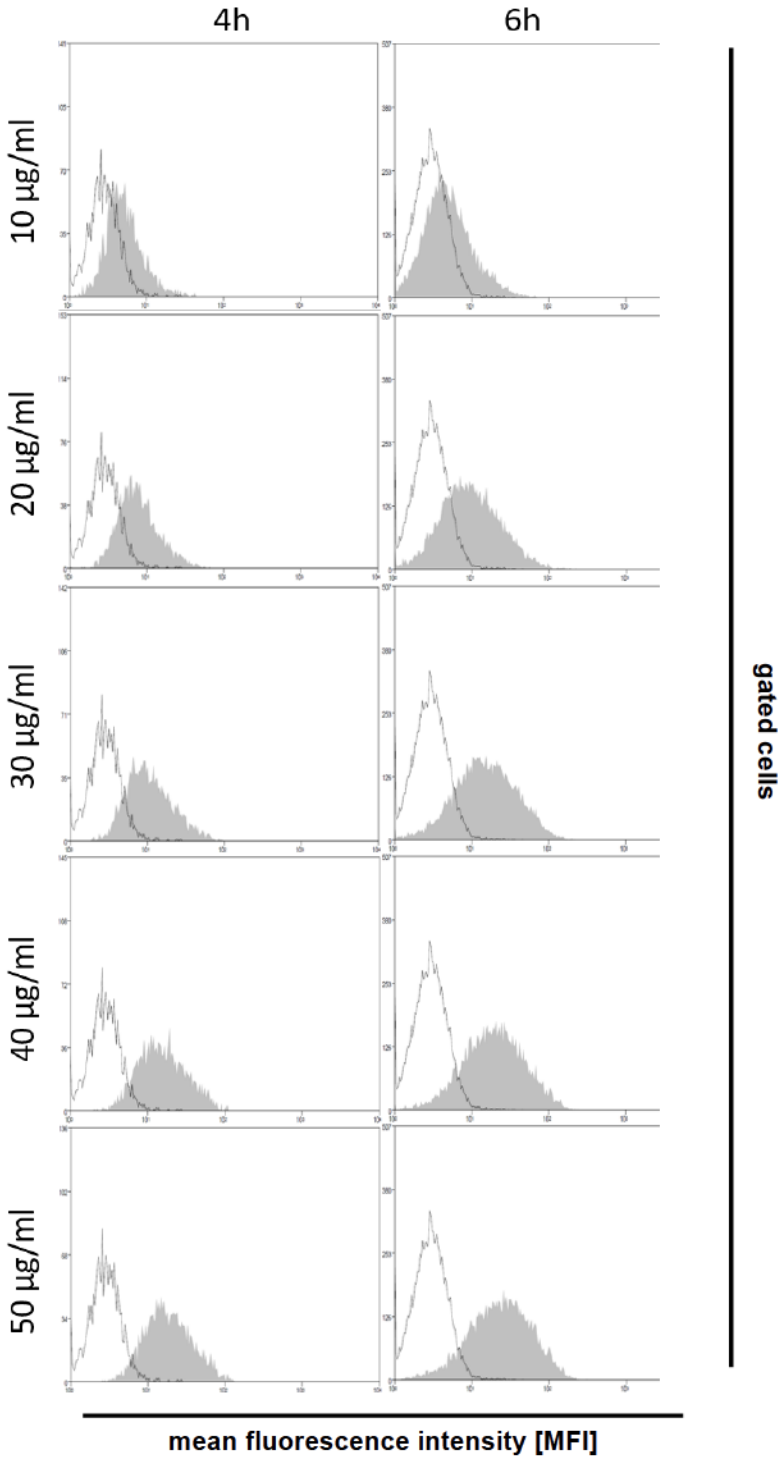

Fig. 5: Representative histogram of PPIX accumulation in U-CH2 cells after 4 h (left column) and 6 h (right column) 5-ALA incubation time.
Flow cytometry was used to measure PPIX accumulation after 5-ALA incubation for different doses. Untreated cells (clear histogram) are shown as comparative group to experimental groups (grey histogram); x-axis: mean fluorescence intensity , y-axis: gated cells.(Cornelius et al. 2017 (100))

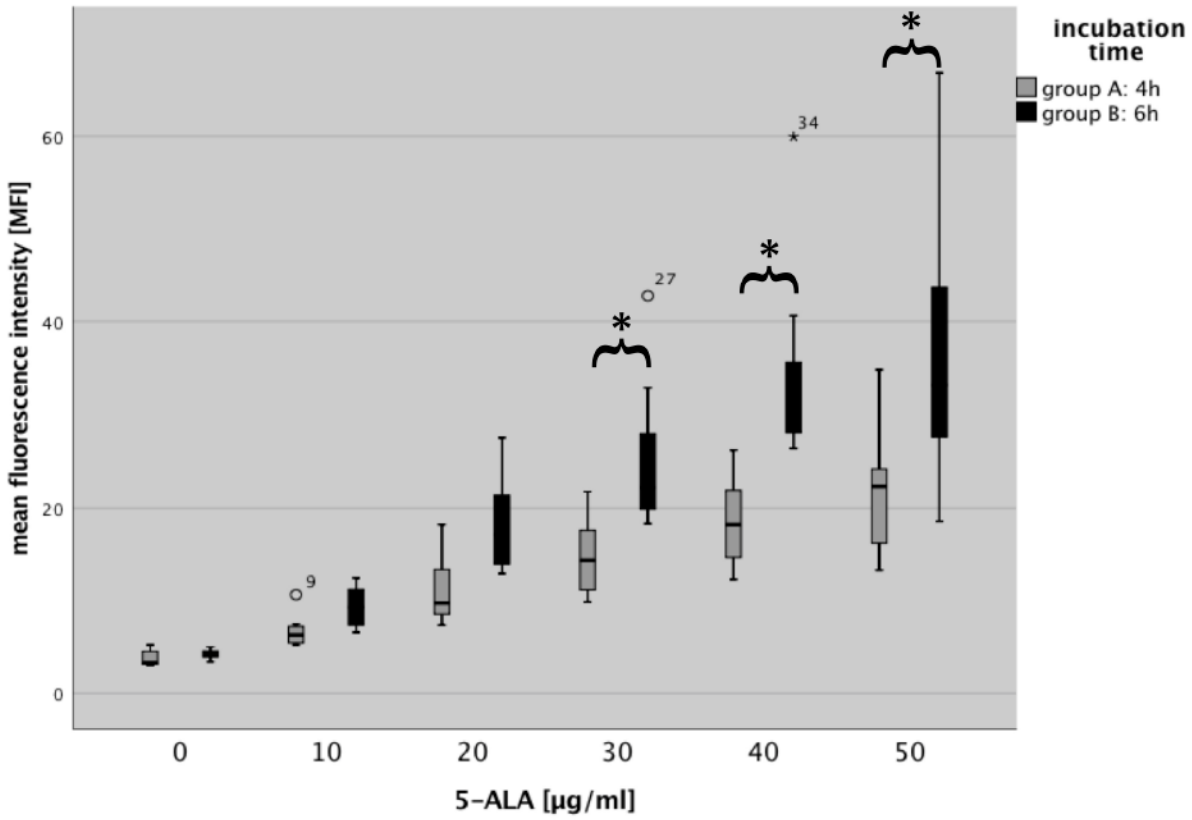

Fig. 6: Mean fluorescence intensity (MFI) of accumulated PPIX after 4 h (grey box plots) and 6 h (black box plots) 5-ALA incubation time.
Seven independent experiments were performed using 5-ALA doses from 10 µg/ml to 50 µg/ml. U-CH2 cells were incubated either for 4 h or for 6 h and following MFI was measured by flow cytometry. Points marked with 9, 27 and 34 are statistical outliers.
* indicates significant difference between experimental group A and B.

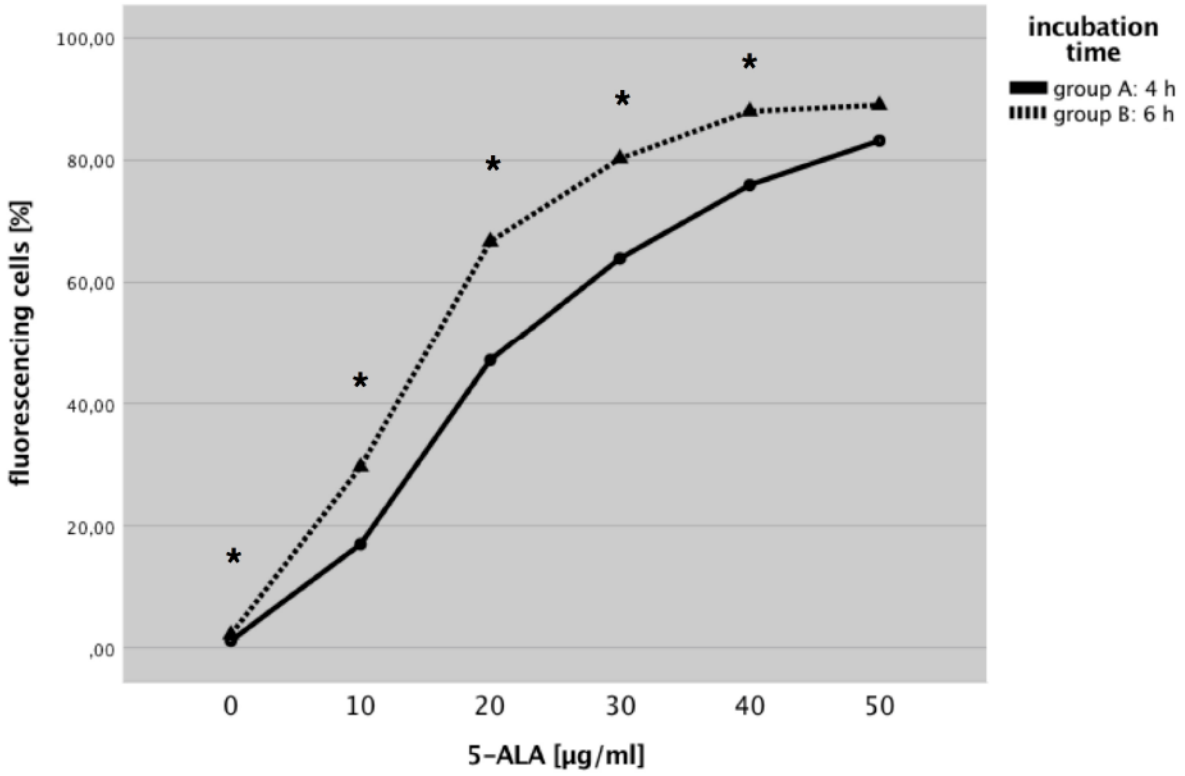

Fig. 7: Mean fractions of fluorescing cells after incubation of graded 5-ALA doses for 4 h and 6 h (n=7).
Fraction of fluorescing U-CH2 cells was detected after 5-ALA incubation time of 4 h (continuous line) and 6 h (discontinuous line) by flow cytometry.
* indicates significant difference between experimental group A and B.

4.2 ALA/PDT efficacy on chordoma U-CH2 cells

There were two experimental groups: one group with low cell density (group C, 15.000 cells/well) and one group with high cell density (group D, 30.000 cells/well). Based on our findings of superior PPIX accumulation after prolonged incubation time we incubated chordoma U-CH2 cells for ALA/PDT with doses of 15, 30, 40 and 50 µg/ml of 5-ALA for 6 h, respectively. Subsequently, cells were illuminated by laser light of 635 nm wavelength for 625 s. After illumination cells were cultured under standard conditions for 24 h before assessing cell viability.

Fig. 8 shows mean cell viability of both experimental groups 24 h after illumination ($n \geq 6$).

In both experimental groups a dose-dependent decrease of cell viability was observed (ANOVA, $p < 0.0001$). Group D, high cell density was significantly more sensitive to ALA/PDT using concentrations of ≥ 30 µg/ml (ANOVA/Bonferroni $p \leq 0.001$). In lower concentrations, 15 µg/ml of 5-ALA, the decreased cell viability of 30.000 cells/well in comparison to 15.000 cells/well was not significant.

In both experimental groups negative controls were examined with laser irradiation only and 5-ALA only. No significant lethal effect was observed in cells treated with irradiation only. Experiments performed with 50 µg/ml of 5-ALA only showed a cell viability in group D of 91.85 % and group C of 92.66 % after treatment.

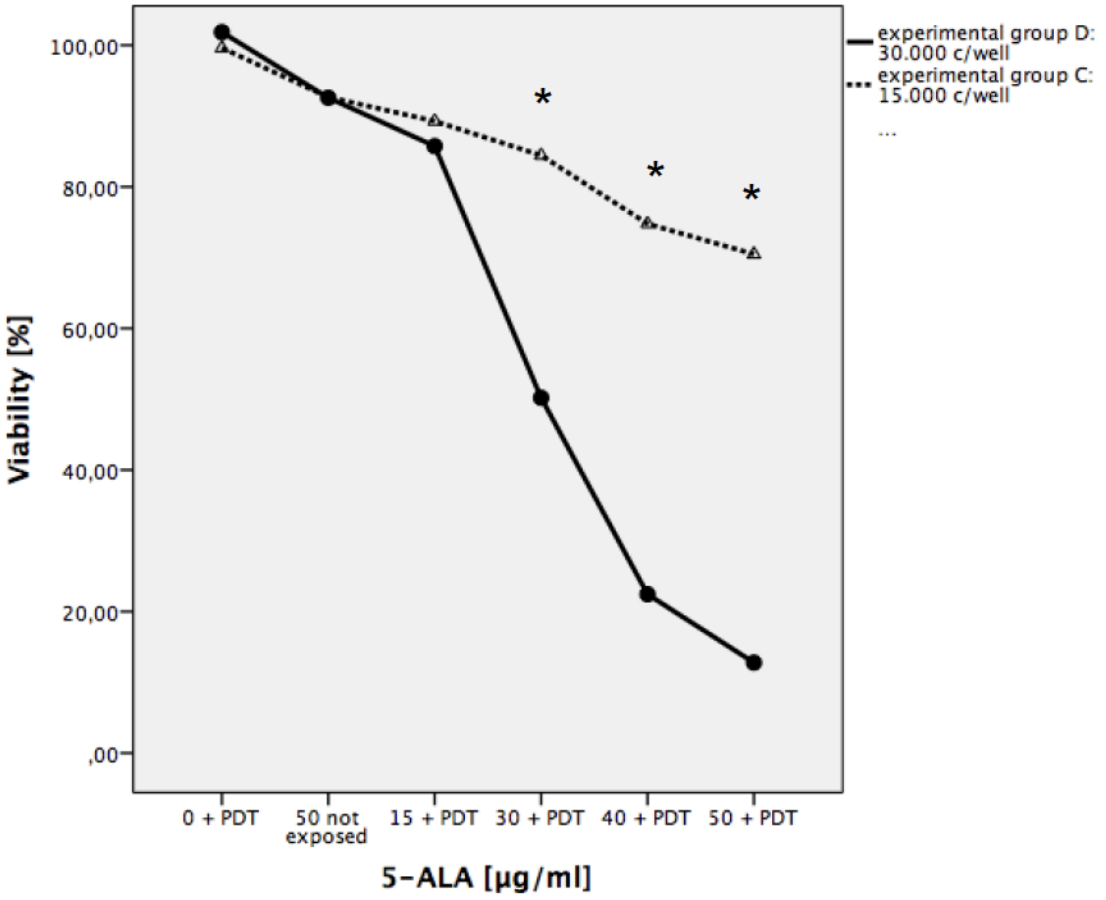

Fig. 8: Mean cellular survival rates of U-CH2 cells treated with different concentrations of ALA/PDT (n≥6).
Experimental groups of 15 000 cells/well (discontinuous line) and 30 000 cells/well (continuous line) showed different sensitivity to ALA/PDT after 6 h incubation time. * indicates significant difference between both experimental groups.

Fig. 9 demonstrates the correlation of MFI to cell survival. A negative linear correlation can be observed of MFI and cell survival ($p < 0.05$; $r^2 = 0.997$).

A light microscopic evaluation was performed before treatment and 24 h after irradiation. **Fig. 10** shows representatives samples of both experimental groups. The image A shows the continuous cell layer of group D before treatment and numerous round configured cells after irradiation in image C. In contrast in image B wide intercellular gaps before treatment of experimental group B can be seen and few normal configured cells after irradiation are shown in image D.

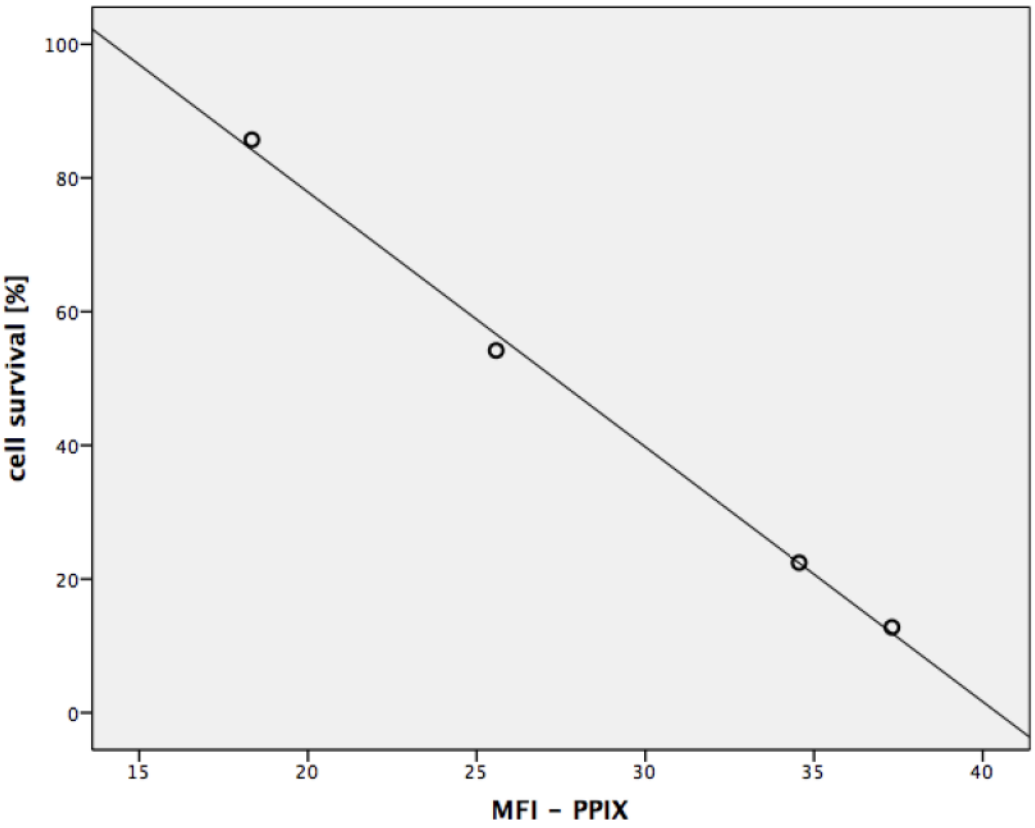

Fig. 9: Mean values of cell survival (group D) in correlation of MFI (group B).
The mean value of ALA/PDT of the group of high cell density (group D) was plotted against the MFI reported after a 6 h incubation time (experimental group B) ($p < 0.05$; $r^2 = 0.997$).

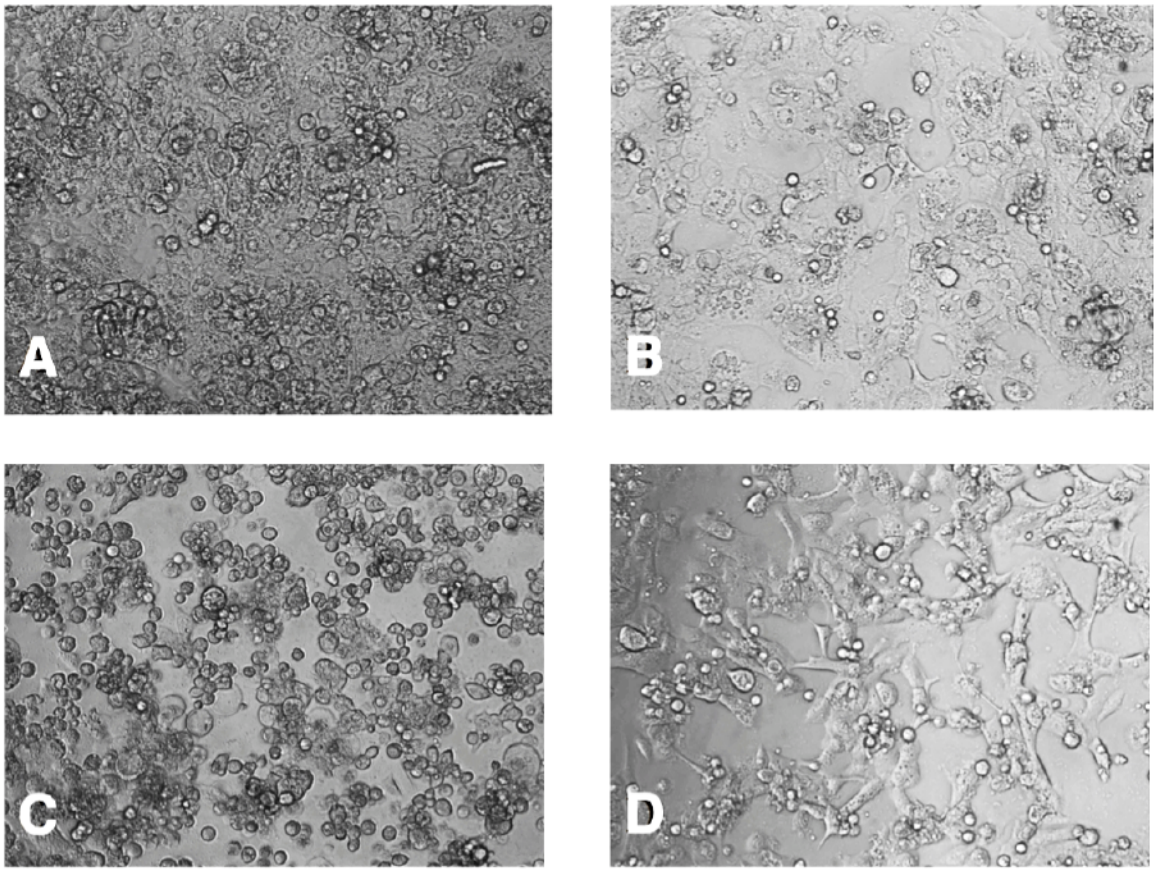

Fig. 10: Light microscopic evaluation of U-CH2 chordoma cells before and 24 h after ALA/PDT (magnification 100-fold, unstained).
A: experimental group of high cell density before ALA/PDT; B: experimental group of low cell density before ALA/PDT; C: experimental group of high cell density 24 h after ALA/PDT; D: experimental group of low cell density 24 h after ALA/PDT. A and B show cell layer before treatment. In A no inter-cellular gap is observed in contrast to B. C shows swollen cells indicating successful cell death after treatment. In D a large fraction of regular configured cells with wide intercellular space remains after treatment.

4.3 Cell cycle Analysis

Chordoma U-CH2 cell's cycle phase was analyzed at the time of cell seeding for ALA/PDT experiments. Therefore, chordoma U-CH2 cells were fixed, stained and cell cycle phase was identified. We found that 75.53 % were in G1/G0-phase, 7.79 % in S-phase and 16.67 % in G2/M-phase. These findings are summarized in **Fig. 11**.

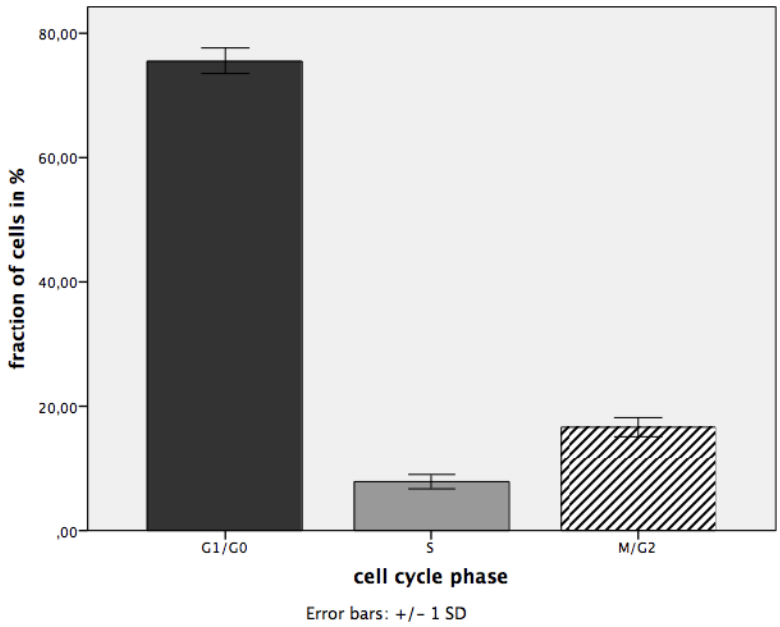

Fig. 11: Mean fractions of cell cycle phase after 8 days of culturing (n=12).
Note: experiments were performed at the same point of time.

5 Discussion

Our study showed that PPIX accumulated dose-dependently in chordoma U-CH2 cells after exogenous 5-ALA application. It was demonstrated that accumulation of 5-ALA after 6 h is superior to commonly used 3-4 h of incubation time for other tumor entities (101-104). Cell survival followed a dose-dependent manner. High cell density in this *in vitro* model was more sensitive to ALA/PDT in comparison to low cell density.

Pharmacokinetic findings

Chordomas are classified as low-grade malignant tumors (8). Slow continuous growth invading functional structures characterizes patient's clinical course (11, 105) and may be responsible for low efficacy of chemotherapy as known in other low-grade malignancies (13). This characteristic growth pattern was observed in the studied chordoma U-CH2 cell line with a relatively long doubling time of 7-8 days in comparison with the mean doubling time of 40 h of the NCI-60 cancer cell lines of *The National Cancer Institute's Developmental Therapeutics Program* which represents a panel of 60 different cancer cell lines (106). Comparable doubling times to

our U-CH2 cell line are also reported in colorectal cancer cell lines ranging from days to weeks (107). Likewise the efficacy of ALA/PDT in an *in vitro* model of a colorectal cancer cell line has been reported (108).

We showed for the first time accumulation of PPIX after exogenous 5-ALA application in chordoma cells and an advantage of prolonged incubation time. Compared to the standard incubation time of 3 h for glioblastoma (86) a prolonged incubation time of 6 h showed significant higher fluorescence in chordoma cells. This was especially observed for higher 5-ALA concentrations in the present study. Cellular conversion of 5-ALA to PPIX appears to be comparatively slow as the general growth pattern of chordomas. An advantage of extended 5-ALA incubation time was also reported in meningioma for higher 5-ALA doses (56) and also in bladder tumor cells with better PDT outcome after 5.5 h of 5-ALA incubation time (109). Also non-malignant human skin fibroblasts revealed a maximum PPIX content after 6 h of incubation time (110). Low malignancies, such as chordomas, might benefit from extended incubation periods in comparison to high-grade, more aggressive neoplasm. Controversially, Iinuma et al. observed in different malignant and non-malignant, cell lines either a decrease or plateau of intracellular PPIX production after 4 h 5-ALA incubation (111). Therefore incubation time must be chosen carefully, because PPIX amount is the result of the dynamic of synthesis and efflux (111). Therefore, our findings are in line with the literature but further investigations are necessary to elucidate the molecular mechanism of synthesis and efflux of intracellular PPIX in chordoma cells.

Cell cycle analysis in U-CH2

Cell cycle analysis showed a large fraction of cells in G1/G0-phase correlating with the slow-growing character of this tumor. Literature is still controversial about influence of cell cycle dependence in photodynamic therapy.

Fukuda et al. (1993) investigated PPIX accumulation at different stages of cell cycle after 5-ALA application in mammalian cells (112). There was no significant difference reported in between cell cycle phases but a tendency of superior PPIX level in G2-phase (112). Several *in vitro* models confirmed a higher PPIX accumulation in G2- or S-phase after 5-ALA application (113, 114). High proliferation rate was asso-

ciated with increased PPIX production in comparison to dormant cells (115). This might be explained by relative intracellular iron depletion due to up-regulation of DNA synthesizing enzymes, which require iron (113, 114, 116). Therefore, further metabolism of PPIX to heme is competing with cell growth (113, 116, 117). Accordingly, cells treated in an *in vitro* model with ALA/PDT were more sensitive in G2/M-phase (113, 116).

On the other hand, recent experiments on a prostate cell line showed that cells in G0/G1-phase accumulate more PPIX and were more sensitive to PDT after exogenous 5-ALA application because of favourable ratio of 5-ALA importer and PPIX exporter expression (118).

In accordance to the mentioned hypothesis we demonstrated that the chordoma cell line U-CH2 with a mean fraction of 75.53 % in G0/G1-phases were highly sensitive to ALA/PDT.

Influence of cell density

Cell size and cell density vary in relationship to cell cycle phase. Cell size which is at a maximum in G2- and M-phase correlates positively with PPIX fluorescence after 5-ALA incubation (119). This might be explained by a large cytoplasm containing the two rate limiting enzymes which contribute highly to PPIX accumulation (119). Thus, typical physaliferous chordoma cells might hold high enzymatic capacity with a cellular diameter of 50 µm and are relatively large in comparison to other malignant cells like urothelial carcinoma where 5-ALA fluorescence is well established (120, 121).

Also, our investigation of ALA/PDT efficacy suggests high influence of cell density and intercellular communication. We found a significantly increased toxic effect after ALA/PDT in experimental groups of high cell density in comparison to low density. Similar observation have already been described in PDT of other cells (70). One hypothesis is based on decreased mitosis rate due to contact inhibition (70). The stinted energy is available for intracellular metabolism processes and increases PPIX production (70). Subsequently, higher PPIX accumulation leads to increased sensitivity of PDT.

Another influencing factor for the effectiveness of photodynamic therapy could be indirect cell death of non-targeted or non-irradiated cells. Indirect cell death in PDT is known and different approaches were undertaken to understand this phenomenon. First described in radiation therapy (122), the so-called bystander effect was transferred to photodynamic treatment (123, 124). The bystander effect is mediated by two different signalling pathways: via gap junctions and/or through medium (125). Gap junctions have been reported to be important in inducing cell death in neighbouring cells of irradiated cells (124). Gap junctions are formed in between narrow neighbouring cells through tunnel proteins to allow direct communication (124). ROS might be one molecule to provide cell death via gap junction but short half life time limits it influence diameter (126).

Studies using α-particle radiation have reported changes of the p53/p21^{WAF1} pathway transmitting its effect via gap junction to bystander cell (127).

Furthermore, nitric oxide (NO) and calcium have been reported to diffuse to bystander cell and induce cell death (124, 126). In PDT NO is formed in target cells and expands quickly to bystander cells and induces apoptosis (124).

In the literature also a delayed bystander effect is described which is mediated via calcium and starts with leakage of endoplasmatic reticulum (ER) and disturbance of calcium homeostasis in irradiated cells (124). Subsequently, a calcium wave reaches the bystander cell via gap junctions and induces NO production and apoptosis (124).

Additionally, the special cellular characteristics of chordoma cells of a tightly formation of mitochondria and ER, called the mitochondria-associated ER membrane (MAM) (2, 128) might support calcium mediated signalling pathways.

Our findings of extended cell death in the high cell density group might be well explained by variously mediated bystander effect.

Future clinical applications

The results of the present study indicate potential usefulness of 5-ALA for fluorescence-guided resection and photodynamic treatment of chordomas.

Chordomas still present a complex pathology with unsatisfying adjuvant treatment options and outcome. Symptoms usually occur at large tumor volume resulting in late diagnosis (15). Subjectively, 37 % of patients report a delayed diagnosis (129). Despite radical surgery, sometimes performed by multiple approaches, local recurrence is frequent and overall survival still limited (15). The current concepts of adjuvant therapy consisting primarily of proton-therapy has improved the dismal prognosis, but needs further improvement.

Fluorescence-guided surgery of chordomas

Administration of 5-ALA prior to surgery could be useful for fluorescence-guided surgery of chordomas. Based on our *in vitro* model a prolonged incubation time of 6 h seems to be favourable in comparison to high malignant glioma C6 cells where *in vitro* experiments describe already a plateau phase after 85 mins incubation time (130). In clinical settings PDD is commonly used for resection of gliomas. Therefore 5-ALA is applied orally 2-4 h prior of anesthesia (86). Further clinical studies are necessary to verify, if orally administered 5-ALA accumulates in chordomas such as in glioblastomas (86). Other characteristics of 5-ALA are expected to be similar: short half-life time in comparison to other PS keeping the risk of dermal photosensitization low (131). In fact, 5-ALA plasma concentration is maximum 6.7 h after oral application and less than 5 % remain after 40 h (132). Frequent side-effects are nausea for less than 15 mins and vomiting (131). To avoid skin phototoxicity patients have to be kept light-protected for 24 h (87).

Intraoperatively, after tumor resection, PDD could be used to detect residual tumor cells. In glioblastoma and bladder tumors the introduction of fluorescence-guidance has significantly improved treatment outcomes (86, 133). In classic surgery of glioblastoma a complete resection is achieved in about 36 % of patients whereas fluorescence-guided resection increases the total excision rate to 65 % (86). In urology the detection rate of bladder tumors could be increased from 77 % in regular cystoscopy to 96 % using PDD (133). Fluorescence-guidance might be beneficial since gross total resection in skull base chordoma is achieved only in 71.6 % of the cases (30). In chordomas located along the mobile spine and the os sacrum wide resection

margins are accomplished in 58 % (129). Residual tumor tissue correlates with local recurrence rate and tumor related death (129, 134).

Fluorescence-guidance improves visualization of tumor tissue in contrast to physiological structures (135). Especially, chordomas located in the deep skull base demand a challenging surgical procedure (19). Frequently, tumor is in tight relationship to cranial nerves or vital blood vessels (19, 136). Complication rates for cranial nerve palsy are reported in 8.7 % and injury of internal carotid artery in 2.5 % (137). Postoperative worsening of daily activities is still reported in 10.7 % (137). Therefore, optional live fluorescence imaging would offer additional safety to white light surgery. This might be helpful for surgeons to preserve vital structures, especially in removal of skull base chordoma and to minimize residual tumor tissue.

Intraoperative PDT

Besides better detection another potential clinical application may be an intraoperative therapeutic use of ALA/PDT in chordomas. ALA/PDT could be performed after resection of the tumor to induce cell death in residual tumor cells. After tumor resection the resection cavity could be illuminated by a diode laser to trigger photochemical reaction in PPIX. Even narrow surgical corridors such as endonasal approaches for skull base chordomas could allow insertion of a laser. For other tumor entities balloon techniques are used to allow a homogenous illumination of the resection cavity (138-140).

So far different malignancies in neurosurgery have been described using PDT as adjuvant treatment modality. Marks et al. reported promising results in the use of PDT in recurrent pituitary adenoma which are also located in proximity of vulnerable structures like the optic nerve (141). A small number of patient was treated with surgery and intraoperative PDT (141). The follow-up MRI scan showed reduced tumor volume over 12 months (141).

Furthermore, research has focused on high aggressive tumors such as gliomas introducing PDT as treatment option. A study of 73 patients with glioblastoma reported an improvement of the 2-year survival rate from 7 % with standard therapy to 26.7 % treated with standard therapy and PDT (138).

Also, other surgical specialities have taken advantage of intraoperative PDT. As postoperative tumor residual cause local recurrence of non-small cell lung carcinoma (NSCLC) intraoperative PDT additional to the standard therapy was studied (52). The mean survival of 17.6 months in patients treated with surgery and chemotherapy in comparison to 37 months in patients treated additionally with PDT is reported (52).

Likewise in urology patients with bladder cancer suffer from frequent recurrence with rates varying up to 85 % in the first year after transurethral resection (142). Here the mechanism of high recurrence might also be explained by residual tumor cells (143). Filonenko et al. reports a decrease of relapse after combining TUR and PDT in comparison to monotherapy of TUR in non-muscle invasive bladder carcinoma (142).

Beside using PDT postoperatively some studies have investigated the primary use of interstitial PDT. Therefore the laser diode is placed into the tumor mass for irradiation (144). A recent study of small volume glioblastoma has been treated with interstitial ALA/PDT instead of primary resection both followed by standard adjuvant treatment (145). The results were in favour of interstitial ALA/PDT with a median progression free survival (PFS) of 16 months vs. 10.2 months after resection (145).

Interstitial PDT has also been reported with better outcomes for low risk prostate cancer in comparison with active surveillance (146). As well, promising results were also described for therapy of refractory head and neck tumors which are often in close anatomical relation to vital structures (146).

These clinical results of ALA/PDT or PDT using other PSs in different cancer entities have been promising. PDT has been proved to be a suitable treatment option in malignancies with similar challenges such as high recurrence rates after incomplete resection or difficult surgical access due to proximity of major vessels or nerves.

Based on our first *in vitro* chordoma cell model ALA/PDT holds potential for a variety of future therapy concepts.

6 Limitations and future perspectives

One of the major limitations of ALA/PDT is tissue penetration depth. Penetration of red light laser is about 5 mm (63). The nature of chordomas might allow a deeper penetration due to gelatinous characteristics and physaliferous cells, which are rich of transparent vacuoles (13, 147). Furthermore, based on the observed extended cell death in our *in vitro* model one may hypothesize that the therapeutical effect has a wider range than the pure penetration depth of the laser light.

The presented results provide new and original information about PPIX accumulation and ALA/PDT cell death in the U-CH2 chordoma cell line. The characteristic biological behaviour of this special cell line may influence results. Therefore, further investigation should validate these experiences in different chordoma cell lines and primary tumor tissue.

7 Conclusion

Chordomas are complex tumors of the skull base and sacral region. Their proximity to vital structures and their infiltrating growth make surgical removal difficult. Hence new adjuvant therapy strategies have to be developed. The presented *in vitro* model is the first successful attempt of PDT in chordomas. Other important findings were: 1.) U-CH2 chordoma cells metabolized 5-ALA to PPIX, 2.) PPIX accumulation was optimal after 6 h 5-ALA incubation time, 3.) ALA/PDT had a dose-dependent lethal effect, 4.) high cell density of chordomas increased toxic effect of ALA/PDT as compared to low cell density. In analogy to other tumors PPIX fluorescence in chordomas also holds potential for fluorescence-guided surgery (photodiagnosis, PDD). These preliminary *in vitro* findings are very promising and should be confirmed by further investigations.

References

1. Sen C, Triana AI, Berglind N, Godbold J, Shrivastava RK. Clival chordomas: clinical management, results, and complications in 71 patients. Journal of neurosurgery. 2010;113(5):1059-71.

2. Kolb D, Pritz E, Steinecker-Frohnwieser B, Lohberger B, Deutsch A, Kroneis T, et al. Extended ultrastructural characterization of chordoma cells: the link to new therapeutic options. PloS one. 2014;9(12):e114251.

3. Gulluoglu S, Turksoy O, Kuskucu A, Ture U, Bayrak OF. The molecular aspects of chordoma. Neurosurgical review. 2016;39(2):185-96; discussion 96.

4. Bell D, Raza SM, Bell AH, Fuller GN, DeMonte F. Whole-transcriptome analysis of chordoma of the skull base. Virchows Archiv : an international journal of pathology. 2016.

5. Makhdoomi R, Ramzan A, Khursheed N, Bhat S, Baba K, Mohsin R, et al. Clinicopathological characteristics of chordoma: an institutional experience and a review of the literature. Turkish neurosurgery. 2013;23(6):700-6.

6. Choi D, Gleeson M. Surgery for Chordomas of the Craniocervical Junction: Lessons Learned. Skull Base. 2010;20(01):041-5.

7. Rich TA, Schiller A, Suit HD, Mankin HJ. Clinical and pathologic review of 48 cases of chordoma. Cancer. 1985;56(1):182-7.

8. Sun X, Hornicek F, Schwab JH. Chordoma: an update on the pathophysiology and molecular mechanisms. Current reviews in musculoskeletal medicine. 2015;8(4):344-52.

9. von Witzleben A, Goerttler LT, Lennerz J, Weissinger S, Kornmann M, Mayer-Steinacker R, et al. In chordoma, metastasis, recurrences, Ki-67 index, and a matrix-poor phenotype are associated with patients' shorter overall survival. European spine journal : official publication of the European Spine Society, the European Spinal Deformity Society, and the European Section of the Cervical Spine Research Society. 2015.

10. Colia V, Stacchiotti S. Medical treatment of advanced chordomas. European journal of cancer (Oxford, England : 1990). 2017;83:220-8.

11. Stacchiotti S, Sommer J. Building a global consensus approach to chordoma: a position paper from the medical and patient community. The Lancet Oncology. 2015;16(2):e71-e83.

12. El-Heliebi A, Kroneis T, Wagner K, Meditz K, Kolb D, Feichtinger J, et al. Resolving tumor heterogeneity: genes involved in chordoma cell development identified by low-template analysis of morphologically distinct cells. PloS one. 2014;9(2):e87663.

13. Chugh R, Tawbi H, Lucas DR, Biermann JS, Schuetze SM, Baker LH. Chordoma: the nonsarcoma primary bone tumor. The oncologist. 2007;12(11):1344-50.

14. Youssef C, Aoun SG, Moreno JR, Bagley CA. Recent advances in understanding and managing chordomas. F1000Research. 2016;5:2902.

15. Walcott BP, Nahed BV, Mohyeldin A, Coumans J-V, Kahle KT, Ferreira MJ. Chordoma: current concepts, management, and future directions. The Lancet Oncology. 2012;13(2):e69-e76.

16. Fletcher CD UK, Mertens F. Pathology and Genetics of Tumours of Soft Tissue and Bone. IARC Press. 2002:316-7.

17. Tian K, Wang L, Ma J, Wang K, Li D, Du J, et al. MR Imaging Grading System for Skull Base Chordoma. AJNR Am J Neuroradiol. 2017.

18. Stacchiotti S, Gronchi A, Fossati P, Akiyama T, Alapetite C, Baumann M, et al. Best practices for the management of local-regional recurrent chordoma: a position paper by the Chordoma Global Consensus Group. Annals of Oncology. 2017;28(6):1230-42.

19. Chibbaro S, Cornelius JF, Froelich S, Tigan L, Kehrli P, Debry C, et al. Endoscopic endonasal approach in the management of skull base chordomas--clinical experience on a large series, technique, outcome, and pitfalls. Neurosurgical review. 2014;37(2):217-24; discussion 24-5.

20. Tan NC, Naidoo Y, Oue S, Alexander H, Robinson S, Wickremesekera A, et al. Endoscopic surgery of skull base chordomas. Journal of neurological surgery Part B, Skull base. 2012;73(6):379-86.

21. Justin F. Fraser, Gurston G. Nyquist, Moore N, Vijay K. Anand, Theodore H. Schwartz. Endoscopic endonasal transclival resection of chordomas: operative technique, clinical outcome, and review of the literature. Journal of neurosurgery. 2010;112(5):1061-9.

22. Rahme RJ, Arnaout OM, Sanusi OR, Kesavabhotla K, Chandler JP. Endoscopic Approach to Clival Chordomas: The Northwestern Experience. World Neurosurgery. 2018;110:e231-e8.

23. Colli BO, Al-Mefty O. Chordomas of the skull base: follow-up review and prognostic factors. Neurosurgical Focus. 2001;10(3):1-11.

24. Pendharkar AV, Ho AL, Sussman ES, Desai A. Surgical Management of Sacral Chordomas: Illustrative Cases and Current Management Paradigms. Cureus. 2015;7(8):e301.

25. Sciubba DM, De la Garza Ramos R, Goodwin CR, Xu R, Bydon A, Witham TF, et al. Total en bloc spondylectomy for locally aggressive and primary malignant tumors of the lumbar spine. European spine journal : official publication of the European Spine Society, the European Spinal Deformity Society, and the European Section of the Cervical Spine Research Society. 2016;25(12):4080-7.

26. Arnautovic KI, Al-Mefty O. Surgical seeding of chordomas. Neurosurg Focus. 2001;10(3):E7.

27. Shimony N, Gonen L, Shofty B, Abergel A, Fliss DM, Margalit N. Surgical resection of skull-base chordomas: experience in case selection for surgical

approach according to anatomical compartments and review of the literature. Acta Neurochirurgica. 2017;159(10):1835-45.

28. Fourney DR, Gokaslan ZL. Current management of sacral chordoma. Neurosurg Focus. 2003;15(2):E9.

29. Wang L, Wu Z, Tian K, Wang K, Li D, Ma J, et al. Clinical features and surgical outcomes of patients with skull base chordoma: a retrospective analysis of 238 patients. Journal of neurosurgery. 2017;127(6):1257-67.

30. Tzortzidis F, Elahi F, Wright D, Natarajan SK, Sekhar LN. Patient Outcome at Long-term Follow-up after Aggressive Microsurgical Resection of Cranial Base Chordomas. Neurosurgery. 2006;59(2):230-7.

31. Cloyd JM, Acosta FL, Jr., Polley MY, Ames CP. En bloc resection for primary and metastatic tumors of the spine: a systematic review of the literature. Neurosurgery. 2010;67(2):435-44; discussion 44-5.

32. Radaelli S, Stacchiotti S, Ruggieri P, Donati D, Casali PG, Palmerini E, et al. Sacral Chordoma: Long-term Outcome of a Large Series of Patients Surgically Treated at Two Reference Centers. Spine. 2016;41(12):1049-57.

33. Yang C, Hornicek FJ, Wood KB, Schwab JH, Choy E, Iafrate J, et al. Characterization and analysis of human chordoma cell lines. Spine. 2010;35(13):1257-64.

34. Fleming GF, Heimann PS, Stephens JK, Simon MA, Ferguson MK, Benjamin RS, et al. Dedifferentiated chordoma. Response to aggressive chemotherapy in two cases. Cancer. 1993;72(3):714-8.

35. Chugh R, Dunn R, Zalupski MM, Biermann JS, Sondak VK, Mace JR, et al. Phase II study of 9-nitro-camptothecin in patients with advanced chordoma or soft tissue sarcoma. Journal of clinical oncology : official journal of the American Society of Clinical Oncology. 2005;23(15):3597-604.

36. Arora A, Scholar EM. Role of tyrosine kinase inhibitors in cancer therapy. The Journal of pharmacology and experimental therapeutics. 2005;315(3):971-9.

37. Casali PG, Messina A, Stacchiotti S, Tamborini E, Crippa F, Gronchi A, et al. Imatinib mesylate in chordoma. Cancer. 2004;101(9):2086-97.

38. Stacchiotti S, Marrari A, Tamborini E, Palassini E, Virdis E, Messina A, et al. Response to imatinib plus sirolimus in advanced chordoma. Annals of oncology : official journal of the European Society for Medical Oncology. 2009;20(11):1886-94.

39. Singhal N, Kotasek D, Parnis FX. Response to erlotinib in a patient with treatment refractory chordoma. Anti-Cancer Drugs. 2009;20(10):953-5.

40. Yasuda M, Bresson D, Chibbaro S, Cornelius JF, Polivka M, Feuvret L, et al. Chordomas of the skull base and cervical spine: clinical outcomes associated with a multimodal surgical resection combined with proton-beam radiation in 40 patients. Neurosurgical review. 2012;35(2):171-82; discussion 82-3.

41. Herman D. Suit, Michael Goitein, John Munzenrider, Lynn Verhey, Kenneth R. Davis, Andreas Koehler, et al. Definitive radiation therapy for chordoma and

chondrosarcoma of base of skull and cervical spine. Journal of neurosurgery. 1982;56(3):377-85.

42. Thieblemont C, Biron P, Rocher F, Bouhour D, Bobin JY, Gerard JP, et al. Prognostic factors in chordoma: role of postoperative radiotherapy. European journal of cancer (Oxford, England : 1990). 1995;31a(13-14):2255-9.

43. Di Maio S, Temkin N, Ramanathan D, Sekhar LN. Current comprehensive management of cranial base chordomas: 10-year meta-analysis of observational studies. Journal of neurosurgery. 2011;115(6):1094-105.

44. De Amorim Bernstein K, DeLaney T. Chordomas and chondrosarcomas-The role of radiation therapy. Journal of surgical oncology. 2016;114(5):564-9.

45. Gatfield ER, Noble DJ, Barnett GC, Early NY, Hoole ACF, Kirkby NF, et al. Tumour Volume and Dose Influence Outcome after Surgery and High-dose Photon Radiotherapy for Chordoma and Chondrosarcoma of the Skull Base and Spine. Clinical Oncology. 2018;30(4):243-53.

46. Young VA, Curtis KM, Temple HT, Eismont FJ, DeLaney TF, Hornicek FJ. Characteristics and Patterns of Metastatic Disease from Chordoma. Sarcoma. 2015;2015:517657.

47. Agostinis P, Berg K, Cengel KA, Foster TH, Girotti AW, Gollnick SO, et al. Photodynamic therapy of cancer: an update. CA: a cancer journal for clinicians. 2011;61(4):250-81.

48. Castano AP, Demidova TN, Hamblin MR. Mechanisms in photodynamic therapy: part two—cellular signaling, cell metabolism and modes of cell death. Photodiagnosis and Photodynamic Therapy. 2005;2(1):1-23.

49. Ackroyd R, Kelty C, Brown N, Reed M. The history of photodetection and photodynamic therapy. Photochem Photobiol. 2001;74(5):656-69.

50. T. J. Dougherty GBG, R. Fiel, K. R. Weishaupt, and D. G. Boyle. Photoradiation Therapy. II. Cure of Animal Tumors With Hematoporphyrin and Light. J Natl Cancer Inst. 1975;55:115 - 21.

51. Friedberg JS, Simone CB, Culligan MJ, Barsky AR, Doucette A, McNulty S, et al. Extended pleurectomy/decortication-based treatment for advanced stage, epithelial mesothelioma yielding a median survival of nearly three years. The Annals of thoracic surgery. 2017;103(3):912-9.

52. Shafirstein G, Battoo A, Harris K, Baumann H, Gollnick SO, Lindenmann J, et al. Photodynamic Therapy of Non-Small Cell Lung Cancer. Narrative Review and Future Directions. Annals of the American Thoracic Society. 2016;13(2):265-75.

53. Grant WE, MacRobert A, Bown SG, Hopper C, Speight PM. Photodynamic therapy of oral cancer: photosensitisation with systemic aminolaevulinic acid. The Lancet. 1993;342(8864):147-8.

54. Wenig BL, Kurtzman DM, Grossweiner LI, Mafee MF, Harris DM, Lobraico RV, et al. Photodynamic therapy in the treatment of squamous cell carcinoma of the head and neck. Archives of otolaryngology--head & neck surgery. 1990;116(11):1267-70.

55. Bader MJ, Stepp H, Beyer W, Pongratz T, Sroka R, Kriegmair M, et al. Photodynamic therapy of bladder cancer - a phase I study using hexaminolevulinate (HAL). Urologic oncology. 2013;31(7):1178-83.

56. Cornelius JF, Slotty PJ, El Khatib M, Giannakis A, Senger B, Steiger HJ. Enhancing the effect of 5-aminolevulinic acid based photodynamic therapy in human meningioma cells. Photodiagnosis Photodyn Ther. 2014;11(1):1-6.

57. Muragaki Y, Akimoto J, Maruyama T, Iseki H, Ikuta S, Nitta M, et al. Phase II clinical study on intraoperative photodynamic therapy with talaporfin sodium and semiconductor laser in patients with malignant brain tumors. Journal of neurosurgery. 2013;119(4):845-52.

58. Xu J, Gao J, Wei Q. Combination of Photodynamic Therapy with Radiotherapy for Cancer Treatment. Journal of Nanomaterials. 2016;2016:7.

59. Pogue BW, O'Hara JA, Demidenko E, Wilmot CM, Goodwin IA, Chen B, et al. Photodynamic therapy with verteporfin in the radiation-induced fibrosarcoma-1 tumor causes enhanced radiation sensitivity. Cancer Res. 2003;63(5):1025-33.

60. Diez B, Ernst G, Teijo MJ, Batlle A, Hajos S, Fukuda H. Combined chemotherapy and ALA-based photodynamic therapy in leukemic murine cells. Leukemia Research. 2012;36(9):1179-84.

61. Peterson CM, Shiah JG, Sun Y, Kopeckova P, Minko T, Straight RC, et al. HPMA copolymer delivery of chemotherapy and photodynamic therapy in ovarian cancer. Advances in experimental medicine and biology. 2003;519:101-23.

62. Snyder JW, Greco WR, Bellnier DA, Vaughan L, Henderson BW. Photodynamic therapy: a means to enhanced drug delivery to tumors. Cancer Res. 2003;63(23):8126-31.

63. Allison RR, Moghissi K. Photodynamic Therapy (PDT): PDT Mechanisms. Clinical endoscopy. 2013;46(1):24-9.

64. Nicolas Fotinos MAC, Florence Popowycz, Robert Gurny and Norbert Lange'. 5-Aminolevulinic Acid Derivatives in Photomedicine Characteristics Application and Perspectives. Photochemistryand Photobiology. 2006;82:994-1 015.

65. Rene´ C. Krieg HM, Joachim Rauch, Stefan Seeger and Ruth Knuechel. Metabolic Characterization of Tumor Cell–specific Protoporphyrin IX Accumulation After Exposure to 5-Aminolevulinic Acid in Human Colonic Cells. Photochemistry and Photobiology. 2002;76(5):518 - 25.

66. Wang J, Xu J, Chen J, He Q, Xiang L, Huang X, et al. Successful photodynamic therapy with topical 5-aminolevulinic acid for five cases of cervical intraepithelial neoplasia. Archives of gynecology and obstetrics. 2010;282(3):307-12.

67. Loh CS, MacRobert AJ, Bedwell J, Regula J, Krasner N, Bown SG. Oral versus intravenous administration of 5-aminolaevulinic acid for photodynamic therapy. Br J Cancer. 1993;68(1):41-51.

68. Hamblin MR. Advances in Photodynamic Therapy: Basic, Translational, and Clinical: Artech House; 2008.

69. Berkovitch-Luria G, Weitman M, Nudelman A, Rephaeli A, Malik Z. Multifunctional 5-aminolevulinic acid prodrugs activating diverse cell-death pathways. Investigational new drugs. 2012;30(3):1028-38.

70. Johan MOAN ØB, Jean-Michel GAULLIER, Trond STOKKE, Harald B. STEEN, LiWei MA and Kristian BERG. Protoporphyrin IX accumulation in cells treated with 5-aminolevulinic acid: dependence on cell density, cell size and cell cycle. Int J Cancer. 1998;75:134 - 9.

71. Plaetzer K, Krammer B, Berlanda J, Berr F, Kiesslich T. Photophysics and photochemistry of photodynamic therapy: fundamental aspects. Lasers in medical science. 2009;24(2):259-68.

72. Wachowska M, Muchowicz A, Firczuk M, Gabrysiak M, Winiarska M, Wańczyk M, et al. Aminolevulinic Acid (ALA) as a Prodrug in Photodynamic Therapy of Cancer. Molecules. 2011;16(5):4140.

73. Dabrowski JM, Arnaut LG. Photodynamic therapy (PDT) of cancer: from local to systemic treatment. Photochemical & photobiological sciences : Official journal of the European Photochemistry Association and the European Society for Photobiology. 2015;14(10):1765-80.

74. Tetard MC, Vermandel M, Mordon S, Lejeune JP, Reyns N. Experimental use of photodynamic therapy in high grade gliomas: a review focused on 5-aminolevulinic acid. Photodiagnosis Photodyn Ther. 2014;11(3):319-30.

75. Marsden VS, Strasser A. Control of apoptosis in the immune system: Bcl-2, BH3-only proteins and more. Annual review of immunology. 2003;21:71-105.

76. Chipuk JE, Bouchier-Hayes L, Green DR. Mitochondrial outer membrane permeabilization during apoptosis: the innocent bystander scenario. Cell death and differentiation. 2006;13(8):1396-402.

77. Bratton SB, Salvesen GS. Regulation of the Apaf-1-caspase-9 apoptosome. Journal of cell science. 2010;123(Pt 19):3209-14.

78. Vanlangenakker N, Berghe T, Krysko D, Festjens N, Vandenabeele P. Molecular Mechanisms and Pathophysiology of Necrotic Cell Death. Current Molecular Medicine. 2008;8(3):207-20.

79. Buytaert E, Dewaele M, Agostinis P. Molecular effectors of multiple cell death pathways initiated by photodynamic therapy. Biochim Biophys Acta. 2007;1776(1):86-107.

80. Altman BJ, Rathmell JC. Metabolic stress in autophagy and cell death pathways. Cold Spring Harb Perspect Biol. 2012;4(9):a008763.

81. Hong-Tai Ji L-TC, Yu-Hsin Lin, Hsiung-Fei Chien and Chin-Tin Chen. 5-ALA mediated photodynamic therapy induces autophagic cell death via AMP-activated protein kinase. Molecular Cancer. 2010;9(91).

82. Peng Q, Nesland JM. Effects of Photodynamic Therapy on Tumor Stroma. Ultrastructural Pathology. 2004;28(5-6):333-40.

83. Dolmans DEJGJ, Kadambi A, Hill JS, Waters CA, Robinson BC, Walker JP, et al. Vascular Accumulation of a Novel Photosensitizer, MV6401, Causes Selective Thrombosis in Tumor Vessels after Photodynamic Therapy. Cancer Research. 2002;62(7):2151.

84. Etminan N, Peters C, Lakbir D, Bunemann E, Borger V, Sabel MC, et al. Heat-shock protein 70-dependent dendritic cell activation by 5-aminolevulinic acid-mediated photodynamic treatment of human glioblastoma spheroids in vitro. Br J Cancer. 2011;105(7):961-9.

85. Celli JP, Spring BQ, Rizvi I, Evans CL, Samkoe KS, Verma S, et al. Imaging and photodynamic therapy: mechanisms, monitoring, and optimization. Chemical reviews. 2010;110(5):2795-838.

86. Stummer Wea. Fluorescence-guided surgery with 5-aminolevulinic acid for resection of malignant glioma: a randomised controlled multicentre phase III trial. Lancet Oncol. 2006 May;7(5 , 392 - 401).

87. Tonn JC, Stummer W. Fluorescence-guided resection of malignant gliomas using 5-aminolevulinic acid: practical use, risks, and pitfalls. Clinical neurosurgery. 2008;55:20-6.

88. Kim A, Khurana M, Moriyama Y, Wilson BC. Quantification of in vivo fluorescence decoupled from the effects of tissue optical properties using fiber-optic spectroscopy measurements. Journal of Biomedical Optics. 2010;15(6):067006.

89. Cornelius JF, Slotty PJ, Kamp MA, Schneiderhan TM, Steiger HJ, El-Khatib M. Impact of 5-aminolevulinic acid fluorescence-guided surgery on the extent of resection of meningiomas--with special regard to high-grade tumors. Photodiagnosis Photodyn Ther. 2014;11(4):481-90.

90. Coluccia D, Fandino J, Fujioka M, Cordovi S, Muroi C, Landolt H. Intraoperative 5-aminolevulinic-acid-induced fluorescence in meningiomas. Acta Neurochir (Wien). 2010;152(10):1711-9.

91. Valdes PA, Bekelis K, Harris BT, Wilson BC, Leblond F, Kim A, et al. 5-Aminolevulinic Acid-Induced Protoporphyrin IX Fluorescence in Meningioma: Qualitative and Quantitative Measurements In Vivo. Neurosurgery. 2014;10(0 1):74-83.

92. Stummer W, Rodrigues F, Schucht P, Preuss M, Wiewrodt D, Nestler U, et al. Predicting the "usefulness" of 5-ALA-derived tumor fluorescence for fluorescence-guided resections in pediatric brain tumors: a European survey. Acta Neurochir (Wien). 2014;156(12):2315-24.

93. Barbagallo GM, Certo F, Heiss K, Albanese V. 5-ALA fluorescence-assisted surgery in pediatric brain tumors: report of three cases and review of the literature. Br J Neurosurg. 2014;28(6):750-4.

94. Agawa Y, Wataya T. The use of 5-aminolevulinic acid to assist gross total resection of pediatric astroblastoma. Child's nervous system : ChNS : official journal of the International Society for Pediatric Neurosurgery. 2018;34(5):971-5.

95. Kamp MA, Fischer I, Buhner J, Turowski B, Cornelius JF, Steiger HJ, et al. 5-ALA fluorescence of cerebral metastases and its impact for the local-in-brain progression. Oncotarget. 2016;7(41):66776-89.

96. Kamp MA, Grosser P, Felsberg J, Slotty PJ, Steiger HJ, Reifenberger G, et al. 5-aminolevulinic acid (5-ALA)-induced fluorescence in intracerebral metastases: a retrospective study. Acta Neurochir (Wien). 2012;154(2):223-8; discussion 8.

97. Utsuki S, Miyoshi N, Oka H, Miyajima Y, Shimizu S, Suzuki S, et al. Fluorescence-guided resection of metastatic brain tumors using a 5-aminolevulinic acid-induced protoporphyrin IX: pathological study. Brain tumor pathology. 2007;24(2):53-5.

98. Hu Y, Masamune K. Flexible laser endoscope for minimally invasive photodynamic diagnosis (PDD) and therapy (PDT) toward efficient tumor removal. Opt Express. 2017;25(14):16795-812.

99. Bruderlein S, Sommer JB, Meltzer PS, Li S, Osada T, Ng D, et al. Molecular characterization of putative chordoma cell lines. Sarcoma. 2010;2010:630129.

100. Cornelius JF, Eismann L, Ebbert L, Senger B, Petridis AK, Kamp MA, et al. 5-Aminolevulinic acid-based photodynamic therapy of chordoma: In vitro experiments on a human tumor cell line. Photodiagnosis and Photodynamic Therapy. 2017;20:111-5.

101. Teshigawara T, Mizuno M, Ishii T, Kitajima Y, Utsumi F, Sakata J, et al. Novel potential photodynamic therapy strategy using 5-Aminolevulinic acid for ovarian clear-cell carcinoma. Photodiagnosis Photodyn Ther. 2018;21:121-7.

102. El-Khatib M, Tepe C, Senger B, Dibue-Adjei M, Riemenschneider MJ, Stummer W, et al. Aminolevulinic acid-mediated photodynamic therapy of human meningioma: an in vitro study on primary cell lines. International journal of molecular sciences. 2015;16(5):9936-48.

103. Schwake M, Nemes A, Dondrop J, Schroeteler J, Schipmann S, Senner V, et al. In-Vitro Use of 5-ALA for Photodynamic Therapy in Pediatric Brain Tumors. Neurosurgery. 2018:nyy054-nyy.

104. Fisher CJ, Niu C, Foltz W, Chen Y, Sidorova-Darmos E, Eubanks JH, et al. ALA-PpIX mediated photodynamic therapy of malignant gliomas augmented by hypothermia. PloS one. 2017;12(7):e0181654-e.

105. Song PH, Beyhaghi H, Sommer J, Bennett AV. Symptom burden and life challenges reported by adult chordoma patients and their caregivers. Quality of Life Research. 2017;26(8):2237-44.

106. Ross DT, Scherf U, Eisen MB, Perou CM, Rees C, Spellman P, et al. Systematic variation in gene expression patterns in human cancer cell lines. Nature genetics. 2000;24(3):227-35.

107. Farrell TM, Pettengill OS, Longnecker DS, Cate CC, Cohn KH. Growing colorectal tumors: minimizing microbial and stromal competition and assessing in vitro selection pressures. Cytotechnology. 2000;34(3):205-11.

108. Hatakeyama T, Murayama Y, Komatsu S, Shiozaki A, Kuriu Y, Ikoma H, et al. Efficacy of 5-aminolevulinic acid-mediated photodynamic therapy using light-emitting diodes in human colon cancer cells. Oncology reports. 2013;29(3):911-6.

109. Bachor R, Reich, E., Rück, A. et al. Aminolevulinic acid for photodynamic therapy of bladder carcinoma cells. Urol Res. 1996(0300-5623 (Print)).

110. Zhou BR, Zhang LC, Permatasari F, Liu J, Xu Y, Luo D. ALA-PDT elicits oxidative damage and apoptosis in UVB-induced premature senescence of human skin fibroblasts. Photodiagnosis and Photodynamic Therapy June 2016;14(1873-1597 (Electronic)):47-56.

111. Iinuma S, Farshi SS, Ortel B, Hasan T. A mechanistic study of cellular photodestruction with 5-aminolaevulinic acid-induced porphyrin. British Journal of Cancer. 1994;70(1):21-8.

112. Fukuda H, Batlle AMC, Riley PA. Kinetics of porphyrin accumulation in cultured epithelial cells exposed to ALA. International Journal of Biochemistry. 1993;25(10):1407-10.

113. Wyld L, Smith O, Lawry J, Reed MW, Brown NJ. Cell cycle phase influences tumour cell sensitivity to aminolaevulinic acid-induced photodynamic therapy in vitro. British Journal of Cancer. 1998;78(1):50-5.

114. Li N, Sun M, Wang Y, Lv Y, Hu Z, Cao W, et al. Effect of cell cycle phase on the sensitivity of SAS cells to sonodynamic therapy using low-intensity ultrasound combined with 5-aminolevulinic acid in vitro. PloS one. 2015(1791-3004 (Electronic)).

115. Schick E, Kaufmann R Fau - Ruck A, Ruck A Fau - Hainzl A, Hainzl A Fau - Boehncke WH, Boehncke WH. Influence of activation and differentiation of cells on the effectiveness of photodynamic therapy. Acta Derm Venereol. 1995;75(4)(0001-5555 (Print)):276-9.

116. Rittenhouse-Diakun K, Van Leengoed H Fau - Morgan J, Morgan J Fau - Hryhorenko E, Hryhorenko E Fau - Paszkiewicz G, Paszkiewicz G Fau - Whitaker JE, Whitaker Je Fau - Oseroff AR, et al. The role of transferrin receptor (CD71) in photodynamic therapy of activated and malignant lymphocytes using the heme precursor delta-aminolevulinic acid (ALA). Photochem Photobiol. 1995;61(5)(0031-8655 (Print)):523-8.

117. Hryhorenko EA, Rittenhouse-Diakun K Fau - Harvey NS, Harvey Ns Fau - Morgan J, Morgan J Fau - Stewart CC, Stewart Cc Fau - Oseroff AR, Oseroff AR. Characterization of endogenous protoporphyrin IX induced by delta-aminolevulinic acid in resting and activated peripheral blood lymphocytes by four-color flow cytometry. Photochem Photobiol 1998;67(5)(0031-8655 (Print)):565-72.

118. Nakayama T, Otsuka S, Kobayashi T, Okajima H, Matsumoto K, Hagiya Y, et al. Dormant cancer cells accumulate high protoporphyrin IX levels and are sensitive to 5-aminolevulinic acid-based photodynamic therapy. 2016;6:36478.

119. Gibbs SL, Chen B Fau - O'Hara JA, O'Hara Ja Fau - Hoopes PJ, Hoopes Pj Fau - Hasan T, Hasan T Fau - Pogue BW, Pogue BW. Protoporphyrin IX level

correlates with number of mitochondria, but increase in production correlates with tumor cell size. Photochem Photobiol. 2006;82(5)(0031-8655 (Print)):1334-41.

120. Friedmann I, Harrison DFN, Bird ES. The fine structure of chordoma with particular reference to the physaliphorous cell. Journal of Clinical Pathology. 1962;15:116-25.

121. Keshtkar A, Keshtkar A, Lawford P. Cellular morphological parameters of the human urinary bladder (malignant and normal). International Journal of Experimental Pathology. 2007;88(3):185-90.

122. Najafi M, Fardid R, Hadadi G, Fardid M. The Mechanisms of Radiation-Induced Bystander Effect. Journal of Biomedical Physics & Engineering. 2014;4(4):163-72.

123. Kessel DH, Olivier D, Douilard S, Patrice T. PDT-induced in vitro bystander effect. 2009;7380:73803Y.

124. Calì B, Ceolin S, Ceriani F, Bortolozzi M, Agnellini AHR, Zorzi V, et al. Critical role of gap junction communication, calcium and nitric oxide signaling in bystander responses to focal photodynamic injury. Oncotarget. 2015;6(12):10161-74.

125. Bazak J, Fahey JM, Wawak K, Korytowski W, Girotti AW. Enhanced aggressiveness of bystander cells in an anti-tumor photodynamic therapy model: Role of nitric oxide produced by targeted cells. Free Radical Biology and Medicine. 2017;102(Supplement C):111-21.

126. Klammer H, Mladenov E, Li F, Iliakis G. Bystander effects as manifestation of intercellular communication of DNA damage and of the cellular oxidative status. Cancer Letters. 2015;356(1):58-71.

127. Azzam EI, de Toledo SM, Little JB. Oxidative metabolism, gap junctions and the ionizing radiation-induced bystander effect. Oncogene. 2003;22(45):7050-7.

128. Erlandson RA, Tandler B, Lieberman PH, Higinbotham NL. Ultrastructure of Human Chordoma. Cancer Research. 1968;28(10):2115.

129. Bergh P, Kindblom L-G, Gunterberg B, Remotti F, Ryd W, Meis-Kindblom JM. Prognostic factors in chordoma of the sacrum and mobile spine. Cancer. 2000;88(9):2122-34.

130. Stummer W, Stocker S, Novotny A, Heimann A, Sauer O, Kempski O, et al. In vitro and in vivo porphyrin accumulation by C6 glioma cells after exposure to 5-aminolevulinic acid. Journal of photochemistry and photobiology B, Biology. 1998;45(2-3):160-9.

131. Webber J, Kessel D Fau - Fromm D, Fromm D. Side effects and photosensitization of human tissues after aminolevulinic acid. J Surg Res 1997. 1997;68(1)(0022-4804 (Print)).

132. Rick K, Sroka R Fau - Stepp H, Stepp H Fau - Kriegmair M, Kriegmair M Fau - Huber RM, Huber Rm Fau - Jacob K, Jacob K Fau - Baumgartner R, et al. Pharmacokinetics of 5-aminolevulinic acid-induced protoporphyrin IX in skin and blood. J Photochem Photobiol B 1997;40(3)(1011-1344 (Print)):313-9.

133. Jocham D, Witjes F, Wagner S, Zeylemaker B, van Moorselaar J, Grimm M-O, et al. Improved detection and treatment of bladder cancer using hexaminolevulinate imaging: a prospective, phase III multicenter study. The Journal of Urology. 2005;174(3):862-6.

134. Ruggieri P, Angelini A, Ussia G, Montalti M, Mercuri M. Surgical Margins and Local Control in Resection of Sacral Chordomas. Clinical Orthopaedics and Related Research®. 2010;468(11):2939-47.

135. Nguyen QT, Tsien RY. Fluorescence-guided surgery with live molecular navigation — a new cutting edge. 2013;13:653.

136. Labidi M, Watanabe K, Bouazza S, Bresson D, Bernat AL, George B, et al. Clivus chordomas: a systematic review and meta-analysis of contemporary surgical management. J Neurosurg Sci. 2016;60(4):476-84.

137. Zoli M, Milanese L, Bonfatti R, Faustini-Fustini M, Marucci G, Tallini G, et al. Clival chordomas: considerations after 16 years of endoscopic endonasal surgery. Journal of neurosurgery. 2017:1-10.

138. Lyons M, Phang I, Eljamel S. The effects of PDT in primary malignant brain tumours could be improved by intraoperative radiotherapy. Photodiagnosis Photodyn Ther. 2012;9(1):40-5.

139. Wilson BC, Muller PJ, Yanch JC. Instrumentation and light dosimetry for intra-operative photodynamic therapy (PDT) of malignant brain tumours. Physics in medicine and biology. 1986;31(2):125-33.

140. Dupont C, Mordon S, Deleporte P, Reyns N, Vermandel M. A novel device for intraoperative photodynamic therapy dedicated to glioblastoma treatment. Future oncology (London, England). 2017;13(27):2441-54.

141. Marks PV, Belchetz PE, Saxena A, Igbaseimokumo U, Thomson S, Nelson M, et al. Effect of photodynamic therapy on recurrent pituitary adenomas: clinical phase I/II trial ' an early report. British Journal of Neurosurgery. 2000;14(4):317-25.

142. Filonenko EV, Kaprin AD, Alekseev BYa, Apolikhin OI, Slovokhodov EK, Ivanova-Radkevich VI, et al. 5-Aminolevulinic acid in intraoperative photodynamic therapy of bladder cancer (results of multicenter trial). Photodiagnosis and Photodynamic Therapy. 2016;16:106-9.

143. Bryan RT, Collins SI, Daykin MC, Zeegers MP, Cheng KK, Wallace DMA, et al. Mechanisms of recurrence of Ta/T1 bladder cancer. Annals of The Royal College of Surgeons of England. 2010;92(6):519-24.

144. Stepp H, Stummer W. 5-ALA in the management of malignant glioma. Lasers in surgery and medicine. 2018.

145. Schwartz C, Rühm A, Tonn J-C, Kreth S, Kreth F-W. SURG-25INTERSTITIAL PHOTODYNAMIC THERAPY OF DE-NOVO GLIOBLASTOMA MULTIFORME WHO IV. Neuro-Oncology. 2015;17(Suppl 5):v219-v20.

146. Shafirstein G, Bellnier D, Oakley E, Hamilton S, Potasek M, Beeson K, et al. Interstitial Photodynamic Therapy—A Focused Review. Cancers. 2017;9(2):12.

147. Erdem E, Angtuaco EC, Van Hemert R, Park JS, Al-Mefty O. Comprehensive Review of Intracranial Chordoma. RadioGraphics. 2003;23(4):995-1009.

Liste of tables

Liste of figures

Danksagung (Acknowledgement)

An dieser Stelle möchte ich all jenen danken, die durch ihre fachliche und persönliche Unterstützung zum Gelingen dieser Arbeit beigetragen haben.

Ein ganz besonderer Dank gilt dabei Herrn Professor Hans-Jakob Steiger für das Vertrauen und die Möglichkeit diese Arbeit umzusetzen.

Im Speziellen möchte ich mich bei Herrn Priv.-Doz. Dr. med. Jan Frederick Cornelius für das Überlassen des interessanten Themas dieser Dissertation und die Einführung in das wissenschaftliche Arbeiten bedanken. Er hatte jederzeit ein offenes Ohr für meine Fragen während der Arbeit im Labor, der Vorbereitung für den DGNC und zuletzt bei der Bearbeitung der Niederschrift.

Bei wem ich mich ebenfalls in diesem Rahmen nochmals herzlichst bedanken möchte, ist Frau Brigitte Senger, die durch Ihr unermüdliches Engagements und Ihre stetige Unterstützung maßgeblich zum Erfolg dieser Arbeit beigetragen hat. Neben der exzellenten Einführung in die laboratorische Arbeit bekam ich von Ihr viele weitere Kompetenzen für meinen beruflichen und privaten Werdegang mit auf den Weg.

Zudem möchte ich mich für die Zusammenarbeit mit Herrn Priv.-Doz. Dr. rer. nat. Rüdiger Sorg, Frau Lara Ebbert und dem gesamten Team des ITZ der Heinrich Heine Universität Düsseldorf bedanken. Sie standen mir jederzeit mit all Ihren Fertigkeiten und Kenntnissen zur Seite.

Von ganzem Herzen möchte ich mich bei meiner Familie, meinen Freunden und Kommilitonen bedanken, die mich durch die gesamte Promotion begleiteten haben. Hervorheben möchte ich die außerordentliche Unterstützung meiner Schwester Sabine, die mir allzeit einen starken Rückhalt gab.